Quantification of Linear and Nonlinear Energy Transfer Processes in a Plane Wake

by

Isam M. Janajreh

Thesis submitted to the Faculty of the

Virginia Polytechnic Institute and State University

in partial fulfillment of the requirements for the degree of

Master of Science

in

Engineering Science and Mechanics

APPROVED:

Dr. M. Hajj, Chairman

Dr. S. Ragab

Dr. D. Mook

Dr. H. Tieleman

August, 1994

Blacksburg, Virginia

Quantification of Linear and Nonlinear Energy Transfer Processes in a Plane Wake

by

Isam M. Janajreh

Dr. M. Hajj, Chairman

Engineering Science and Mechanics

(ABSTRACT)

The transition to turbulence of plane wakes is characterized by the development of the velocity-fluctuation field from a spectrum of weak random background noise in the initial laminar wake to a nearly featureless broad spectrum of intense fluctuations within the turbulent wake. This transition has also been described as a sequence of instabilities and wave-wave interactions. In the initial small-amplitude stage, a narrow, but continuous, band of dominant instability modes centered near the most unstable mode, known also as the fundamental mode, grow exponentially at rates that can be calculated from the linearized Navier-Stokes equations. As these modes grow, the nonlinear terms become more important and cannot be neglected anymore. The effect of these terms is to introduce wave-wave interactions that lead to quadratic energy transfer between the different spectral components of the velocity-fluctuation field. While the consequences of these interactions, such as broadening of the power spectra, have been observed in many experiments, the characteristics of these interactions have only been examined in limited cases. Previous measurements of the auto-bispectrum showed that three-wave interaction processes are important in the transitioning wake. However, quantification of these processes can only be obtained from measurement of the nonlinear energy transfer rates resulting from the nonlinear wave-wave interactions. Such quantification is very important for understanding the effects of the different mechanisms involved in the transition and final breakdown to turbulence. An understanding of these

mechanisms and their effects can then be used to control the transition by enhancing certain mechanisms and reducing the role of others through external excitation. In this work, quantitative estimates of the auto-bispectrum, linear and quadratic coupling coefficients and the resulting energy transfer rates between the interacting waves at different locations are presented in controlled and natural transitions of the plane wake. The results show that, in both natural and controlled transitions, the underlying nonlinear dynamics are similar. Basically, nonlinear interactions between the instability modes result in energy transfer to harmonic bands as well as low-frequency difference components. These components play an important role in the transfer of energy to the sidebands and the valleys between the peaks. The results also show that, while energy-transfer rates in natural transition are lower than in controlled transition, the random nature of wave excitation in natural transition causes energy transfer to a band of low-frequency components which leads to energy transfer to many sidebands and results in a spectrum that differs dramatically from the one obtained in the controlled case where two instabilities are excited.

Acknowledgements

Great gratitude is due to my advisor Dr. Muhammad R. Hajj. Without his supervision this work would not have materialized. Special appreciation to Dr. D. Mook, Dr. S. Ragab, and Dr. H. Tieleman for their contributions as committee members and for constructive comments. Thanks also to Dr. R. Miksad and Dr. E. Powers from the University of Texas at Austin for their help in providing the data and many helpful comments.

Thanks also to my colleagues Dr. A. Abdelnaser and Mr. Reza Karkehabadi for all the support and fun over the last year. Special thanks are extended to my fiancee Diane and my brother Ibrahim for their love, support and understanding during my study.

Table of Contents

List of Illustrations

Chapter I

Introduction

The transition to turbulence in plane wakes can be described in terms of the development of the velocity-fluctuation field from a narrow spectrum characterized by weak and random background fluctuations in the laminar wake to a broad spectrum of intense fluctuations in the turbulent wake. Between the laminar and turbulent states, the power spectra are characterized by the presence of well defined peaks that represent coherent (wave-like) instability modes. These modes include the most unstable (fundamental) mode, its harmonics and low-frequency components. All of these modes are related to the formation and breakdown of the vortex street in the wake. Analytical treatment of the transition process has been limited to the initial stage of the transition where the energy content of the spectral modes is low. Linear stability analysis, which solve the linearized hydrodynamics equations, has been very successful in predicting growth rates and dispersion characteristics of amplified modes. Furthermore, there has been significant advances in the analysis of secondary instabilities. However, beyond this initial stage, the generation of the harmonic bands, and the low-frequency components

are related to the formation of the vortex street, to variations in the spacings between its elements, and finally to its breakdown. The harmonic bands and low-frequency components gain their energy via nonlinear wave-wave interaction mechanisms. Gaining an understanding of the relative role of each of these mechanisms is an important step towards developing an understanding of the transition process and attempting to control it.

Several experimental and theoretical studies examined the role nonlinear wave-wave interactions could play in the transition of plane wake. The experiments of Sato [1970], Sato & Saito [1975] and Motohashi [1979] indicated that nonlinear interactions result in variations of the characteristics of the fluctuations in the wake. Gertsenshtein, Sukhorukov, and Shkadov [1977], in a theoretical study, showed that low-frequency modulations of the instability fluctuations play an important role in energy transfer to the sidebands. These results have been confirmed experimentally by Miksad et al. [1982] who, using complex demodulation techniques, showed that amplitude modulation plays an important role in providing energy and that phase modulation dominates the spectrum-broadening and energy redistribution process. Auto-bicoherence measurements by the same authors showed that sideband structures and the accompanying modulations are produced by nonlinear coupling between the low-frequency difference mode and high-frequency instability mechanisms. Ritz et al. [1988] presented measurements of quadratic transfer functions and identified different types of nonlinear couplings. The above results have provided new and useful information about the nonlinear interaction mechanisms that govern the transition. However, many fundamental questions regarding these interactions remain unanswered. Classical power spectra show only the consequences of nonlinear wave interactions. Auto-bicoherence measurements have been used to detect wave-wave coupling

mechanisms; however, they do not quantify the direction and magnitude of the energy transfer.

The objective of this study is to quantify the energy-cascading process in the transition to turbulence of a plane wake. This objective is achieved by expressing the governing Navier-Stokes equations in terms of a wave coupling-equation that describes the linear and quadratically nonlinear mechanisms. These mechanisms are represented by the linear and quadratic coupling coefficients. By introducing a finite-difference scheme, the wave-coupling equation is then represented by an input-output system, in which the output contains linear and quadratically nonlinear responses of the input. These responses are represented by linear and quadratic transfer functions. These transfer functions are then determined using the multivariate-analysis technique developed by Kim & Powers [1988]. Measured transfer functions, coupling coefficients along with higher-order spectral moments are then used to determine the linear and quadratic energy-transfer rates.

In Chapter II, a description of the wind tunnel, flow conditions, and data acquisition system is given. In Chapter III, the energy-cascading processes in an acoustically controlled plane wake are quantified. Controlling the transition of the wake makes the interpretation of the results easier than in a "naturally" or randomly excited wake. In Chapter IV, the energy-cascading processes in the natural wake are determined and compared to those in Chapter III. The conclusions of this work are given in chapter V. Methodology used to determine the transfer functions and coupling coefficients is given in appendices A and B.

Chapter II

Experimental Set-Up

The data used in this work was supplied by the nonlinear fluid dynamics laboratory at the University of Texas at Austin. A brief description of the wind tunnel, flow conditions and data acquisition is given in the following two sections.

2.1 Wind-Tunnel Configuration and Flow Conditions

A schematic representation of the wind-tunnel configuration is given in figure 2.1 The wind tunnel is driven by a positive displacement pump from the downstream end. The entry section includes a foam filter, a stilling chamber, two "honeycomb" sections, stainless steel fine-mesh polyster screens, and a contraction zone that has a ratio of 20 to 1. The test section is $20x20x120$ *cm*. An acoustic excitation system is used to excite the instability modes. This system consists of a stereo amplifier, and two speakers

located at the downstream end of the test section. A sonic throat is placed downstream of the test section to reduce the transmission of pump noise into the test section and to control the flow. The piping system at the downstream end contains a resonating filter which can be tuned to eliminate resonant frequency noise. The wake is formed behind a "flat plate" that is made from polished steel and has a maximum thickness of $0.29cm$ and a length of $20.0cm$. The leading-edge shape approximates an ellipse while the trailing edge was tapered to $0.038cm$ to prevent separation. The boundary layer on the plate was determined to be laminar with no primary instability disturbances.

Jones [1983] showed that nonlinear wave-wave interaction mechanisms are most efficient at the cross-stream location of maximum root mean square (*rms*) fluctuation of the streamwise velocity component. All measurements reported in this work were taken at maximum u'_{rms}. The measurements at each location consisted of 512 averages of two-channel velocity data. Each average consisted of 256 data points measured at a sampling rate of $5000Hz$. This gave a frequency resolution $\Delta f = 19.53Hz$.

In the first set of measurements, the flow was excited at two frequencies, $f_1 = 545Hz$ and $f_2 = 580Hz$. The $580Hz$ mode corresponds to the fundamental instability mode observed under natural conditions. The $545Hz$ mode was observed to exhibit high spatial coherence and enhanced growth under natural conditions. Double excitation was used as a means to generate the low-frequency difference mode $f_v = 580 - 545 = 35Hz$. This enabled us to study the interactions between low-frequency and high-frequency modes, which according to Miksad et al. [1982], play an important role in broadening the energy spectrum. In the second set of measurements, no artificial excitation was used. The flow was excited by background noise and is thus referred to as natural transition.

The velocity measurements were taken with two Disa 55M hot-wire anemometer systems. The hot-wire probe has two platinum-coated tungsten-wire elements and is

described in Jones et al. [1988]. Each elements is 5 μm in diameter and 0.1 cm in length. The two wires are separated by 0.15 cm in the spanwise direction and 0.1 cm in the streamwise direction. The experiments were conducted with a free stream velocity of about 8.0 m/s and a turbulence intensity lower than 0.035 percent. Further details of the wind tunnel and instrumentation are given in Jones [1983].

2.2 *Data-Acquisition System*

Simultaneous samples of the signals from the wire elements were obtained using a digital system that consists of a 12-bit LeCroy Datalogger, model 8212A/8, with memory Module 8800/12, and a Programmable Clock, model 8501. The linearized hot-wire signals were DC-filtered by mean of RC filters, and passed through Krohn-Hite anti-aliasing filter set-up at 2.5KHz. All time records in this work were sampled at a rate of 5KHz, with (256x512) sample points length. All spectral computations were performed on RISC/6000 workstations. Contour plots ware obtained using PV-wave (a visual data analysis software) at the Visualization Lab in the Department of Engineering Science and Mechanics.

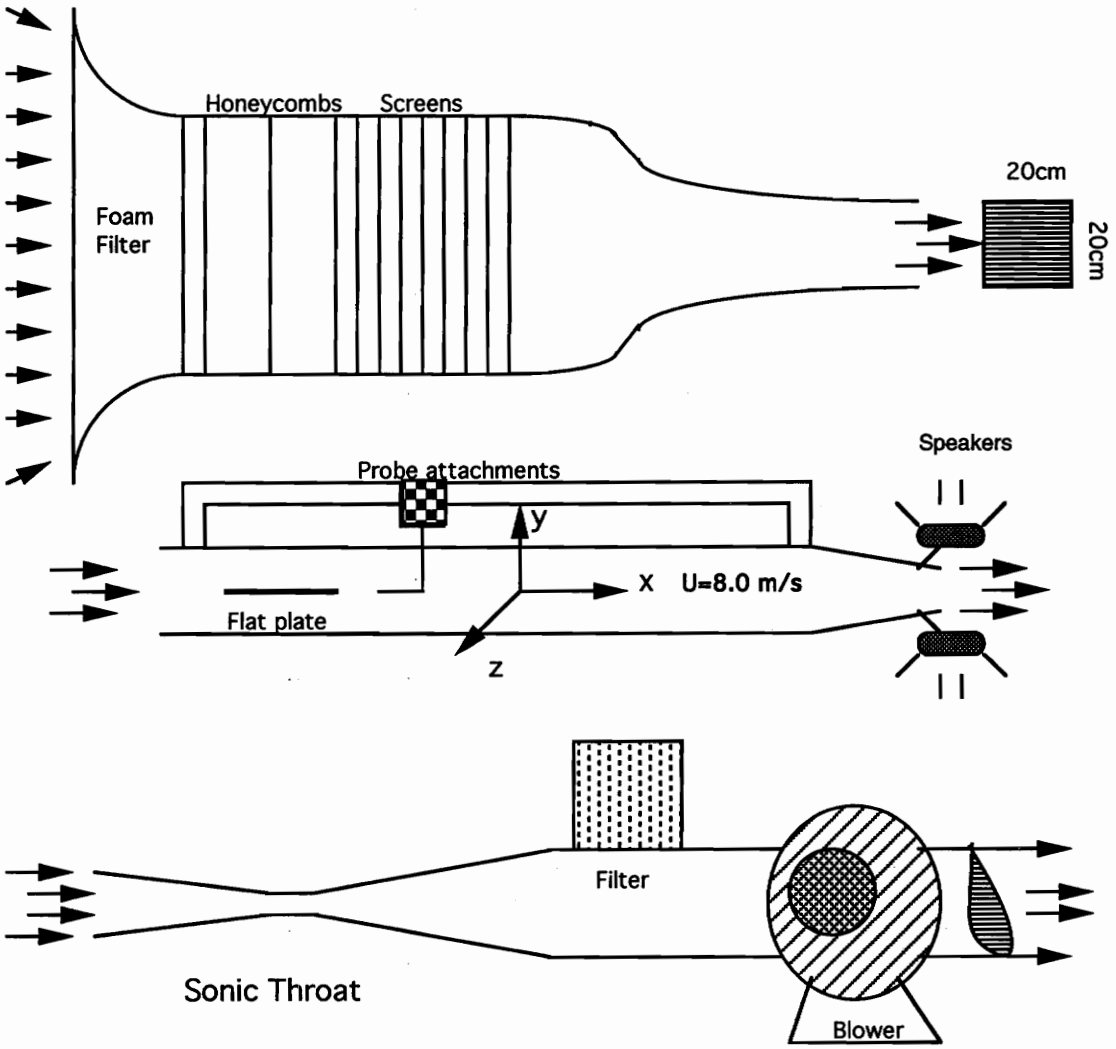

Fig 2.1. A schematic diagram of the different components of the wind-tunnel.

Chapter III

Energy Cascading in a Controlled Wake

The characteristics of the transitioning plane wake are governed by the Navier-Stokes equations. These equations contain quadratically nonlinear terms that determine the rates of energy transfer and redistribution among fluctuating velocity components. Analytical treatment of transitioning flows is currently limited to flow regions where the instability fluctuations are small and where these nonlinear terms can be neglected. The solution of the linearized equations shows that traveling waves within a certain band of frequencies develop and grow with downstream distance. As the level of energy in these modes grows, the quadratic nonlinearties in the Navier-Stokes equations can no longer be neglected since they could result in three-wave couplings, interactions and energy transfer into sum and difference modes.

The experiments of Sato [1970], Sato & Saito [1975] and Motahashi [1979] indicate that nonlinear wave-wave interactions play a dominate role in energy-transfer between the fluctuating components of the transitioning plane wake and in the randomization leading to turbulence. Using complex demodulation techniques to measure amplitude

and phase modulations, Miksad et al. [1982] showed that low-frequency modulations of the instability fluctuations lead to the redistribution of energy into the sidebands of the fundamental mode and its harmonics. These modulations were also described in terms of nonlinear wave-wave interactions between the sidebands and the low-frequency wave. Jones [1983] utilized the classical power spectral and auto-bicoherence measurements in order to characterize the transition process. The results provided new and useful ways of viewing the nonlinear dynamics of the transition. Ritz et al. [1988] presented measurements of quadratic transfer functions and identified types of nonlinear couplings. However, these results did not provide a quantitative measurement of the quadratic energy transfer processes. In order to measure these processes, quantities derived from the governing equations must be determined. Such quantities include the wave-wave coupling coefficients, auto-bispectrum and quadratic energy transfer rates.

The representation of the governing Navier-Stokes equation in terms of a wave coupling equation was given by Kraichnan [1967]. Several transitioning flows have also been represented in terms of wave coupling equations. Nayfeh & Bozatli [1980] described the nonlinear wave-wave interactions in a transitioning boundary layer by a wave-coupling equation. Jones [1983] derived a nonlinear wave-coupling equation for a plane wake and, more recently, Hajj et al. [1992] showed that the fundamental-subharmonic interaction in a plane mixing layer can be examined in terms of nonlinear wave-coupling equations. In general, the nonlinear wave-coupling equation is written as:

$$\frac{\partial \mathrm{X}(f)}{\partial x} = \Lambda_L(f)\mathrm{X}(f) + \sum_{f_i}\sum_{f_j}\Lambda_Q(f_i, f_j)\mathrm{X}(f_i)\mathrm{X}(f_j) \tag{3.1}$$

where $f = f_i \pm f_j$, $X(f)$ is the complex Fourier amplitude with frequency f and ∂x represents the change in the downstream distance. The quantity $\Lambda_L(f)$ is the linear coupling coefficient and is given by:

$$\Lambda_L(f) = \gamma(f) + i\omega(f) \tag{3.2}$$

where $\gamma(f)$ is the linear growth rate and $\omega(f)$ is the dispersion relation of the component with frequency f. The quantity $\Lambda_Q(f_i, f_j)$ is the quadratic coupling coefficient. The contribution of a particular quadratic interaction to the complex Fourier amplitude at frequency f, $X(f)$, is given by the product of the complex Fourier amplitudes, $X(f_i)$ and $X(f_j)$, and the quadratic coupling coefficient $\Lambda_Q(f_i, f_j)$. The intent of this chapter is to examine how the representation of the Navier-Stokes equations in terms of a wave-coupling equation and how measurements of the linear and quadratic coupling coefficients along with higher-order spectral moments enhance our understanding of the linear and nonlinear physics of the controlled transition of a plane wake.

3.1 Spectral Energy Development of The Controlled Wake

In order to characterize the transition process, spectral energy distributions of the velocity fluctuations measured by both upstream and downstream sensors of the probe at several downstream locations are given in figure 3.1. These locations were chosen to cover the different stages of the transition, as proposed by Jones [1983]. All measurements were made at cross-stream locations of maximum u'_{rms} to avoid the

problem of riding up or down an *rms* modal profile. This location was chosen because it coincides with the cross-stream location of maximum u^3_{rms} which, according to bispectral analysis, should mark the location of maximum nonlinear or parametric coupling. The power spectrum at $x = 1.0cm$ shows the emergence of a continuous band of dominant instability modes centered near the excited modes 545Hz and 580Hz. A strong band around the first harmonics of these modes and a relatively weaker band around the second harmonics also appear. The emergence of a peak at $f = 580 - 545 = 35Hz$ is also evident. By $x = 2.0cm$, bands noticed at $x = 1.0cm$, show continuous growth. A new band at the third-harmonics also emerges. By $x = 4.0cm$, the energy of the peaks of the bands at the excited modes and their harmonics start to saturate. Miksad et al. [1987] showed that the Reynolds-stress-production term approaches zero about $x = 6.0cm$ which indicates that by this location, strong energy transfer into the instability modes decreases significantly. Between $x = 8.0cm$ and $x = 35.0cm$, the spectra shows slow filling of the valleys and a shift of energy to low frequencies. By $x = 50.0cm$, the power spectrum has again changed. The characteristics of the spectra indicate that, around this location, the flow is evolving from the vortex street into a nearly turbulent state. By $x = 65cm$, the flow shows a nearly featureless spectrum which characterizes the onset of turbulence.

More information about the characteristics of the different modes in the spectral domain can also be obtained from the plots of linear coherence that are given in figure 3.2. Large coherence values indicate that spectral modes can be treated as coherent waves while low coherence values indicate noisy signals rather than coherent waves. At $x = 1.0cm$, the spatially coherent modes are those with frequencies below 700Hz and those near the first and second harmonics of the excited modes. At $x = 4.0cm$, all modes are highly coherent except for modes in small bands between the second and third harmonics. Further downstream, the spatial coherence in the valleys drops between

$x = 8.0$ and $15.0cm$. A drop in the coherence of the high harmonics peaks is also noticed at $x = 35.0cm$. At $x = 50.0$ and $65.0cm$, all modes show low spatial coherence levels which is a characteristic of the beginning of breakdown to turbulence.

3.2 Linear and Nonlinear Spectral Energy-Cascading Mechanisms

While the classical power spectra presented in figure 3.1 provide a measure of the variations in the character of the fluctuations in the different stages of transition, it is of limited value in trying to quantify the linear growth and nonlinear wave energy-cascading mechanisms that take place and cause these variations. In the following sections, higher-order spectral moments are used to quantify the energy cascading processes. The coefficients defined in equation (3.1), along with other quantities that contain important information regarding the nonlinear stages of transition, are measured. The linear and nolinear physics of the transitioning wake are examined by the use of these measurements. Experimental determination of these coefficients is a major step towards examining the causes and mechanisms of energy cascading and contributes significantly to the theoretical analysis of nonlinear wave-wave interactions in transitioning fluid flows.

Ritz at al. [1989] showed that the change in the spectral power of a wave can be obtained by multiplying the wave-coupling equation, given in (3.1), by $X^*(f)$. A wave kinetic equation that describes the energy transfer can then be written as:

$$\frac{\partial P(f)}{\partial x} = 2\gamma(f)P(f) + \sum_{f_i}^{m}\sum_{f_j}^{m} T(f_i, f_j) \tag{3.3}$$

where

$$P(f) = E[\mathrm{X}(f)\mathrm{X}^*(f)] \tag{3.4}$$

$$T(f_i,f_j) = 2Re\{\Lambda_Q(f_i,f_j).E[\mathrm{X}^*(f)\mathrm{X}(f_i)\mathrm{X}(f_j)]\} \tag{3.5}$$

and E denotes the expected value. Thus the change in the power of a particular component at frequency f can be expressed in terms of the growth rate, $\gamma(f)$, multiplied by the energy content of this component and of the sum of the quadratic coupling coefficients multiplied by the auto-bispectra of all modes that add or subtract to f. Equation 3.5 shows that quadratic energy transfer rate, $T(f_i,f_j)$ is sensitive to the magnitudes as well as the phases of the coupling coefficients and the auto bispectrum. Thus, in order to quantify the energy transfer, one requires measurements of both the coupling coefficients and the auto-bispectrum. The methodology used to determine these quantities is given in appendices A and B. In the following sections, statistical properties, characteristics, measurements and analyses of these quantities are given.

3.2.1 Linear Spectral Energy Transfer

The linear instability mechanisms responsible for energy transfer to the different modes are represented by the growth rate $\gamma(f)$ given in equation (3.3). Figure 3.3 shows the measured growth rates $\gamma(f)$ for all modes below $1000Hz$ at several downstream locations. At $x = 1.0cm$, the results show that spectral modes with frequencies between

$500Hz$ and $620Hz$ have the highest growth rates. These rates vary around $0.26(1/mm)$ which is slightly larger than $0.21(1/mm)$ calculated by Gaster [1965] using linear stability theory. The modes with frequencies between $450Hz$ and $500Hz$ and between $620Hz$ and $700Hz$ show significantly lower growth rates. All modes beyond $700Hz$ show negative growth rates. Moreover modes below $450Hz$ do not show significant growth. These results are in general agreement with the linear stability theory and with Jones [1983]. Further downstream, at $x = 4.0cm$, the modes in the band around the fundamental continue to show enhanced linear growth rates and except for low-frequency modes, all other modes are linearly damped. Beyond $x = 8.0cm$, all modes have negative growth rates.

3.2.2 Nonlinear Spectral Energy-Transfer Mechanisms

The characteristics of the nonlinear energy transfer mechanisms are determined by the use of a sequence of measured quantities that include the auto-bispectrum, quadratic coupling coefficients, and quadratic energy transfer rates.

3.2.2.1 Bispectal Measurements and Analysis

The mathematical background of the bispectrum and the aspects of its applications to nonlinear wave interactions have been discussed by Kim and Powers [1979] and more recently in a review article by Kim and Powers [1994]. The auto-bispectrum $B(f_i, f_j)$ is defined as:

$$B(f_i, f_j) = E[\mathrm{X}(f_i)\mathrm{X}(f_j)\mathrm{X}^*(f)] \tag{3.6}$$

where $f = f_i \pm f_j$, X(f) is the complex Fourier amplitude with frequency f and E denotes an expected value. Kim and Powers [1979] showed that the bispectrum represents the contributions to the mean-cube value by the spectral components at f_i and f_j. If the time series $x(t)$ is real, X($-f$) becomes equal to X*(f) and thus $B(f_i, f_j) = B^*(-f_i, -f_j)$. By summing over all Fourier components, it can be shown that only the real part of the bispectrum contributes to the mean-cube value. Another important aspect of the auto-bispectrum lies in its phase. If the three modes present at f_i, f_j and $f = f_i \pm f_j$ are independent, each mode is characterized by a statistically independent random phase which will result in a near zero value when statistical averaging is carried out. On the other hand, if the three modes present at f_i, f_j and $f_i \pm f_j$ are coupled through a nonlinear or parametric interaction mechanism, a phase coherence will exist among them. Under these conditions, the statistical averaging will not lead to a zero value of the bispectrum. the physics of a given nonlinear or parametric interaction can thus be determined from the characteristics of the measured bispectral quantities. Jones [1983] used a normalized value of the bispectrum, namely, the auto-bicoherence to identify quadratically coupled modes in the transition of a plane wake. The results showed that growing instabilities act to establish a basic harmonic band structure and generate a low-frequency band. These low-frequency fluctuations interact with the harmonic bands to produce a continuous array of sideband fluctuations. These results provided the first quantitative information regarding the nonlinear interaction mechanisms in the plane wake. However, as shown in equation (3.5), bispectral or bicoherence measurements alone do not quantify the energy transfer and redistribution of energy that take place between different modes. Furthermore, such measurements cannot determine whether three-wave coupling is due to interactions occurring at the location where the measurements are taken or are advected past the probe by the flow.

Because the intent of this work is to quantify quadratic energy transfer processes in the transitioning wake and because these processes are dependent on the magnitudes and phases of the auto-bispectrum and the quadratic coupling coefficient, examining the differences between these quantities is essential to understanding of the transition of the plane wake.

As a first step in developing this understanding, two-dimensional plots of the auto-bispectra at several locations in the transitioning wake are shown in figure 3.4. The maximum value of the auto-bispectrum at each of these downstream location is given in table 1. These values are given to provide a basis for comparison between the plots.

Table 1. Auto-bispectrum maximum values

Downstream Location (cm)	Auto-bispectrum ($1/Hz^2$)
1.0	0.011882879
2.0	3.133941414
4.0	1.125817726
8.0	0.123342206
15.0	0.05812729
35.0	0.02975412
50.0	0.00429066
65.0	0.00481914

At $x = 1.0cm$, the highest auto-bispectrum values are at the excited modes and the low-frequency difference mode $f_v = 580 - 545 = 35Hz$. Lower auto-bispectra (by two orders of magnitude) are measured between the first, second and third harmonics. No significant auto-bispectra are measured in the valleys between the peaks. At $x = 2.0cm$, the highest auto-bispectrum values are still noticed at the excited modes and at their harmonics and the difference mode. By $x = 4.0cm$, high levels of the bispectrum continue

to be concentrated at the excited modes, their harmonics and low-frequency difference components. These results show that, between $x = 1.0cm$ and $x = 4.0cm$, the major quadratic coupling mechanism is that between the excited modes. These interactions imply that energy transfer to the harmonics and to the low-frequency difference mode is taking place. However, these measurements do not quantify the magnitude or direction of energy transfer. Furthermore, the measurements do not explain how spectral components in the valleys gain their energy as observed in the power spectra, figure 3.1.

At $x = 8.0cm$, the auto-bispectral measurements continue to stress the coupling between the spectral peaks, i.e. the excited modes, their harmonics and the low-frequency difference modes. It should also be noted that lower level (by three orders of magnitude) auto-bispectral values are measured between modes in the valleys between the first and second peaks. These same observations can be made for $x = 15.0cm$ and $x = 35.0cm$. Again, by comparing the power spectra at $x = 8.0$, 15.0 and $x = 35.0cm$, we note that the energy levels of the valleys have increased significantly. Bispectral measurements do not show high coupling levels between these modes and any of the peaks and thus do not explain the interaction mechanisms that are responsible for the growth of these modes.

At $x = 50.0cm$, we note that high auto-bispectral values are measured between the excited modes and a band of modes between the lowest measured frequency and the excited modes. Lower values (by one order of magnitude) of the auto-bispectra are measured between the low frequencies and the sidebands of the excited modes and their harmonics. One should also note that lower levels are also measured between all spectral components at $x = 65.0cm$, the highest levels of the auto-bispectra are measured between the low-frequency modes, whereas the high-frequency modes showing lower levels of coupling.

Measurements of the auto-bispectra at different locations show that the highest levels of couplings are always detected at the excited modes, their harmonics and low-frequency modes.

3.2.2.2 Quadratic Coupling Coefficient Measurements and Analysis

The methodology used to determine the linear and quadratic coupling coefficients is discussed in appendices A and B. The values of the maximum coupling coefficients at the different downstream locations are given in table 2.

Table 2. Coupling coefficient maximum values

Downstream Location (cm)	Coupling Coefficient (*Hz/mm*)
1.0	6253.14896
2.0	20264.91434
4.0	4813.24539
8.0	4429.90498
15.0	5660.42222
35.0	18621.50518
50.0	39453.21613
65.0	30782.61411

Contour plots of the quadratic coupling coefficients are shown in figure 3.5. At x= 1.0 cm, the contour plots show that the highest quadratic coupling coefficient is that between the low-frequency and the spectral components with frequencies above 700Hz. This is a rather confusing result because power spectral density and auto-bispectra measurements indicate that the harmonics of the excited modes are gaining energy and linear coherence measurements showed that spectral modes with frequency components

above 700Hz are not coherent. The measured highest value of the magnitude of the coupling coefficient thus does not necessarily indicate the highest energy-transfer rate. This is due the sensitivity of the coupling coefficients to the energy level of the input and output modes. By examining the coupling coefficients measurements at the other downstream locations, one can see that the highest coefficients are always measured for pairs of modes with high frequencies (low energy level) and for pairs in the valleys (between the peaks). This stems from the fact that the quadratic coupling coefficient is inversely proportional to the energy level of the interacting modes. That is when the input of interacting modes have high energy level, the coupling coefficients is low and vice versa.

While the quadratic coupling coefficient can be treated as a relevant physical parameter that appears in the governing equation, it must be emphasized that the energy transfer is a function of the phases and magnitudes of the coupling coefficient and auto-bispectrum. Thus, it should not be surprising that the magnitude of the coupling coefficient does not reveal the "true" strength or efficiency of the energy transfer in the transitioning plane wake.

3.2.2.3 Quadratic Energy-Transfer Rates Measurements and Analysis

Energy-transfer rates between the different modes as well as maximum energy-transfer rates vary in the downstream direction. Table 3 show the highest energy-transfer rates between any three modes at the same downstream locations for which the auto-bispectrum and quadratic coupling coefficients were shown. The results show that the highest rates are at $x = 2.0cm$ and $x = 4.0cm$. This is just an indication of the highest quadratic energy transfer between any three modes and does not indicate total quadratic energy transfer.

Table 3. Energy-transfer rate maximum values

Downstream Location (cm)	Energy-Transfer Rate ($1/Hz.mm$)
1.0	-0.00788508
2.0	1.19941666
4.0	-1.03331440
8.0	-0.02514399
15.0	0.04954711
35.0	-0.02288762
50.0	-0.00530478
65.0	0.12668601

Figure 3.6 shows two-dimensional plots of the energy-transfer rates between all spectral components. At $x = 1.0cm$, the highest energy-transfer rate is from the excited modes to their first harmonics, from the excited modes into the low frequency difference mode, and from the fundamental (580Hz) and low-frequency (35Hz) into the sideband (615Hz), the next lower energy-transfer rates are those between the fundamental and the valleys between the excited modes and their first harmonics. The fundamental mode plays a very important role of extracting energy from the mean flow and redistributing it to the harmonics and the valleys. The indications of these measurements differ significantly from those of the bispectra which stress the coupling of the peaks and those of the coupling coefficients which stress the role of low-frequency.

At $x = 2.0cm$, the level of energy-transfer rates increased significantly; the maximum level is $(0.021/Hz.mm)$, compared with a maximum of $(0.00161/Hz.mm)$ measured at $x = 1.0cm$. While the maximum level has increased, it can be noticed that the characteristics of the energy transfer are similar to those obtained at $x = 1.0cm$. By

$x = 4.0cm$, the contours of energy-transfer rates continue to show the largest values at the excited modes and their first harmonics. However new (but not maximum) contours appear between the second, third and fourth harmonics and between the second harmonics and lower frequency modes. These new contours indicate relatively high energy-transfer rates into higher harmonics, their sidebands and the valleys between them. At $x = 8.0cm$, energy transfer is taking place primarily between the fundamental and most other spectral components and between the first harmonic and spectral modes in the valleys. Of particular importance is the low-frequency/high-frequency energy transfer. This is shown in the high contours between the peaks (excited modes and their harmonics) and the low-frequency.

At $x = 35.0cm$ we see further enhancement of the energy transfer between the sidebands representing the cross-sideband interactions. At $x = 50.0cm$ the most significant energy transfer involves the fundamental and the band of modes below the fundamental, and the higher frequencies that cover the full range of spectral modes. These indicates cross-sideband energy transfer. By $x = 65.0cm$, the energy-transfer rates stress an enhancement of the role of the band of modes below the fundamental to transfer energy to a wide band of other spectral components.

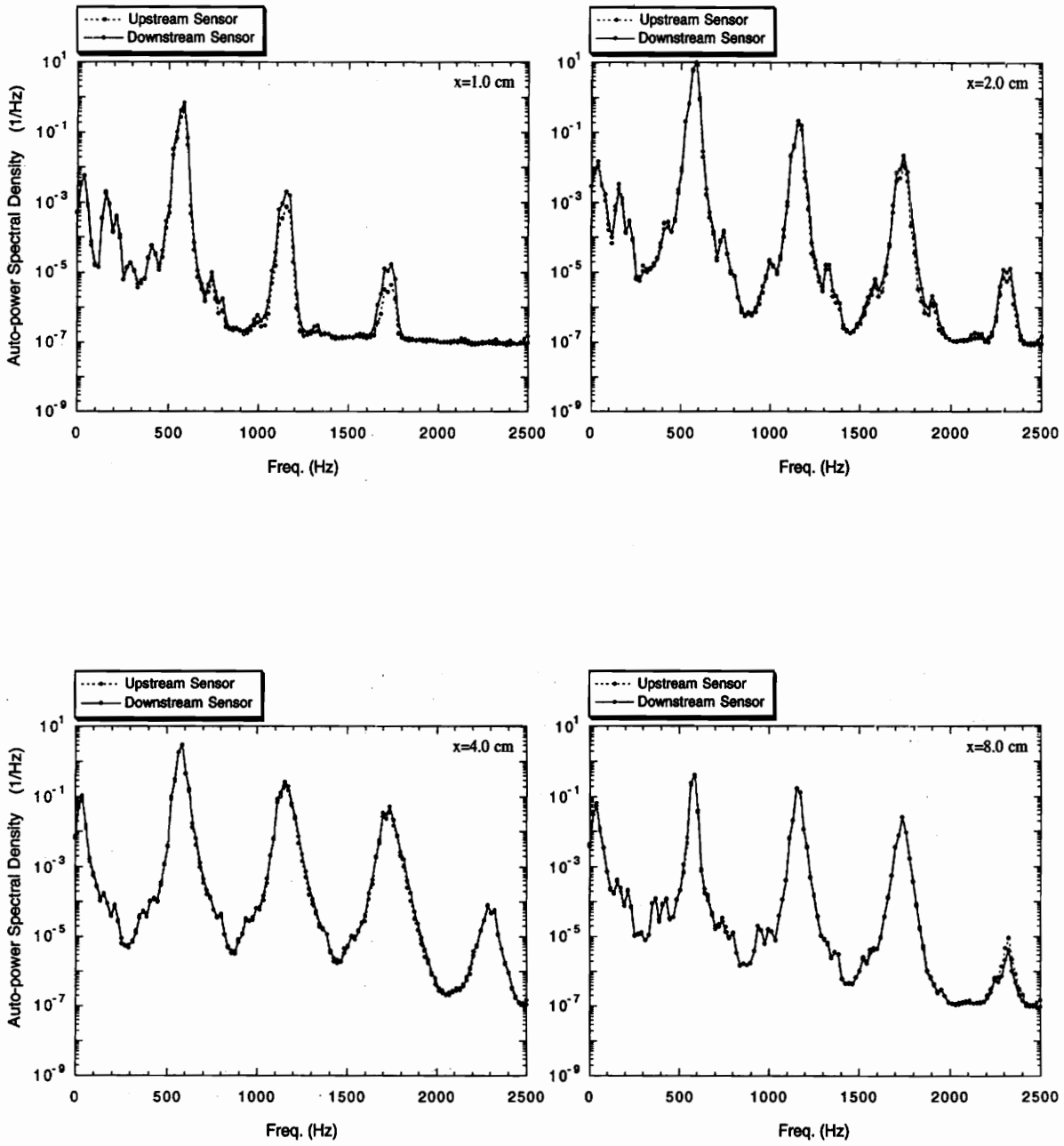

Figure 3.1. Spectral energy distribution of the velocity fluctuations at the cross-stream location of maximum u'_{rms} at x=1.0, 2.0, 4.0, and 8.0cm (controlled case).

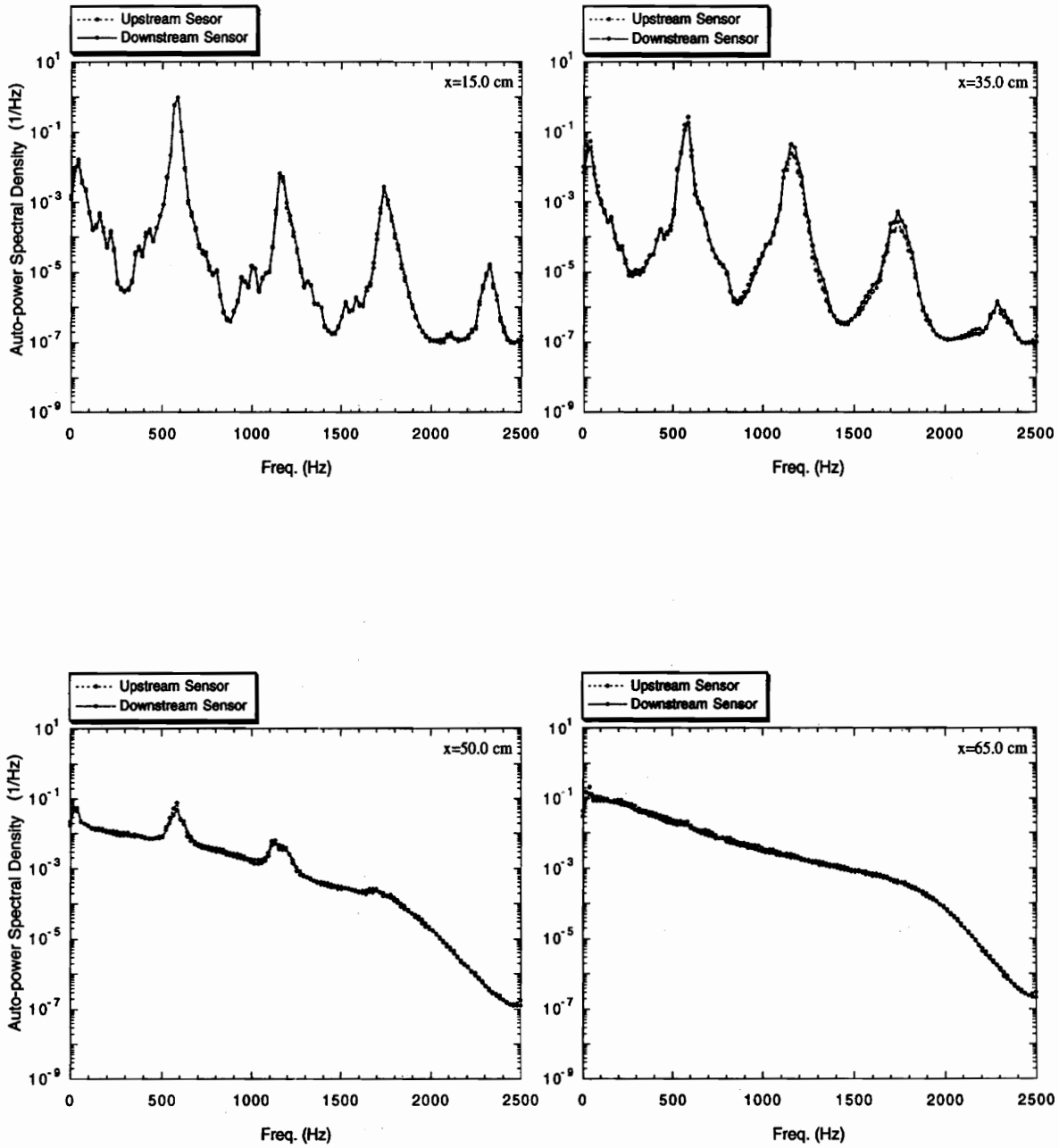

Figure 3.1 (cont'd). Spectral energy distribution of the velocity fluctuations at the cross-stream location of maximum u'_{rms} at x=15.0, 35.0, 50.0, and 65.0cm (controlled case).

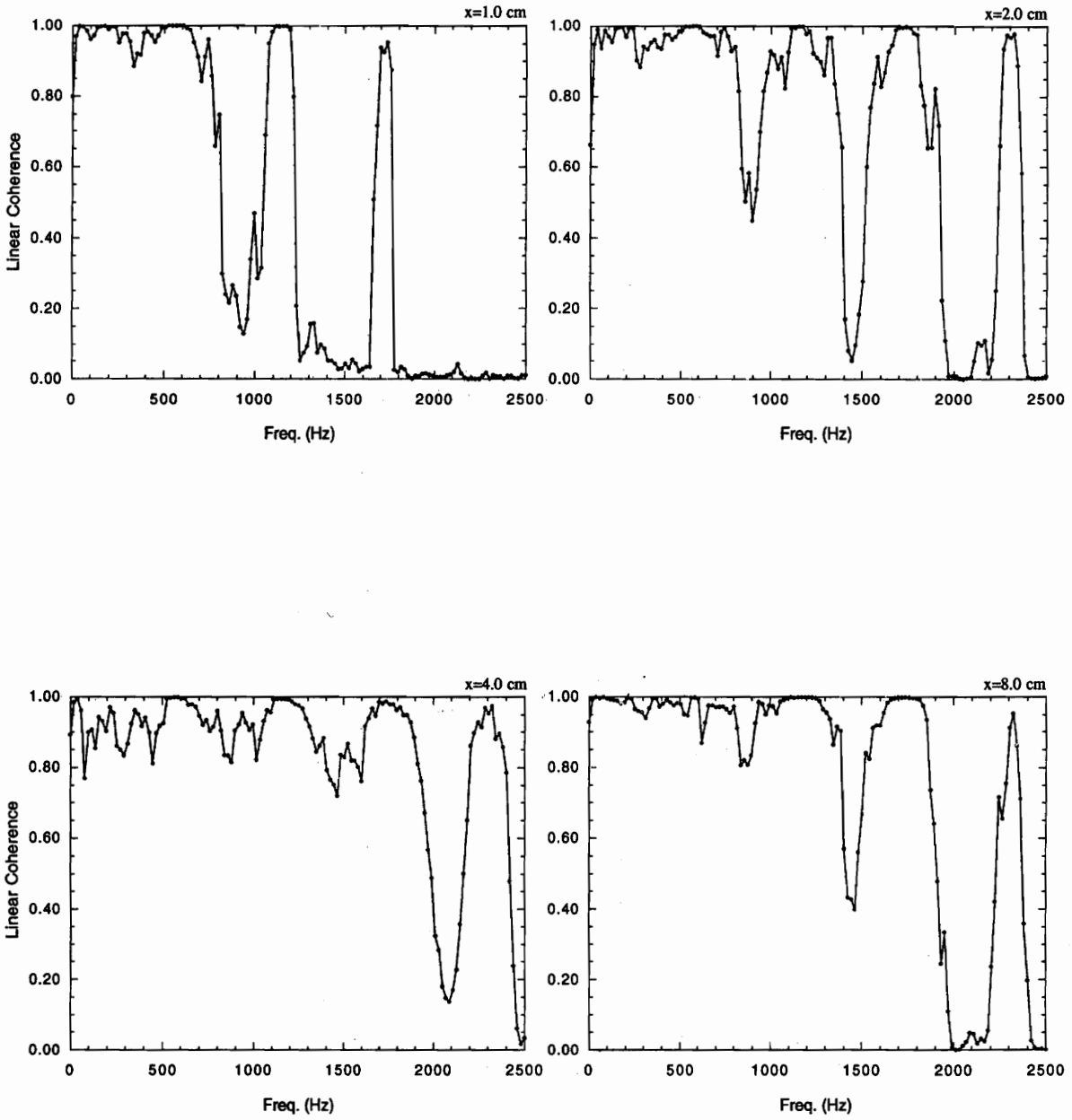

Figure 3.2. Linear coherence between spectral components at the cross-stream location of maximum u'_{rms} at x=1.0, 2.0, 4.0, and 8.0cm (controlled case).

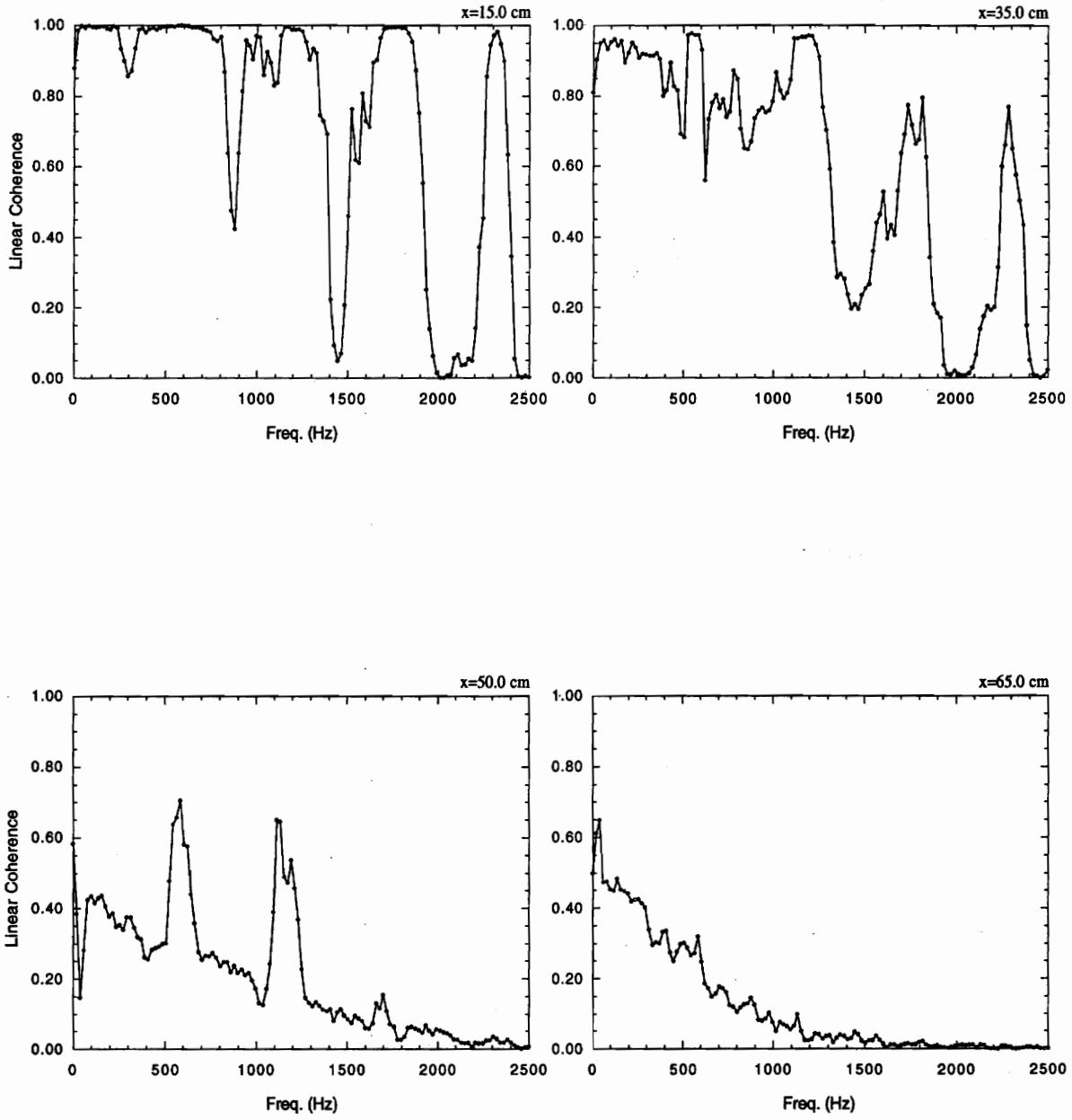

Figure 3.2 (cont'd). Linear coherence between spectral components at the cross stream location of maximum u'_{rms} at x=15.0, 35.0, 50.0, and 65.0cm (controlled case).

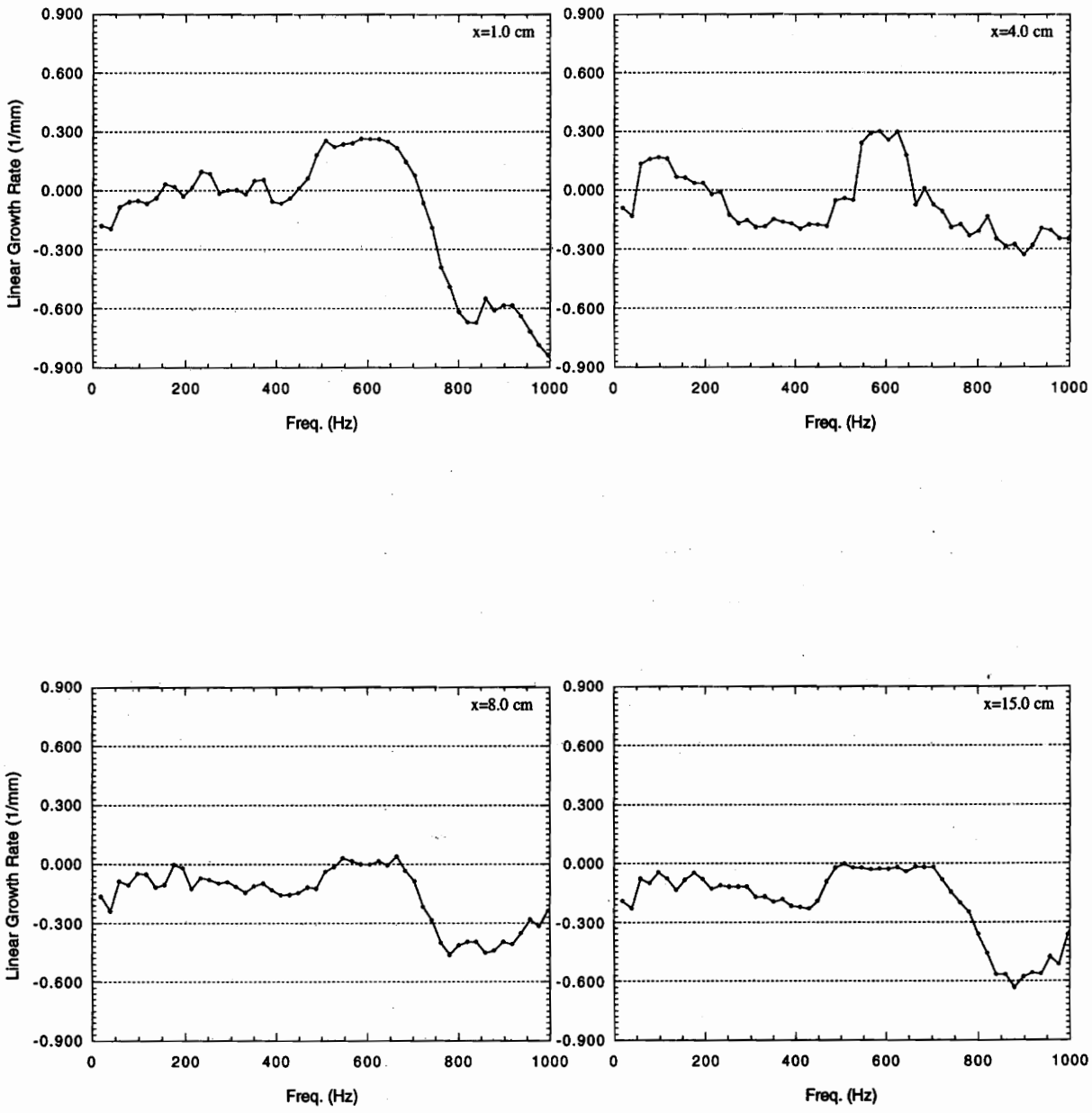

Figure 3.3. Growth rate of the spectral components at the cross-stream location of maximum u'_{rms} at x=1.0, 4.0, 8.0, and 15.0cm (controlled case).

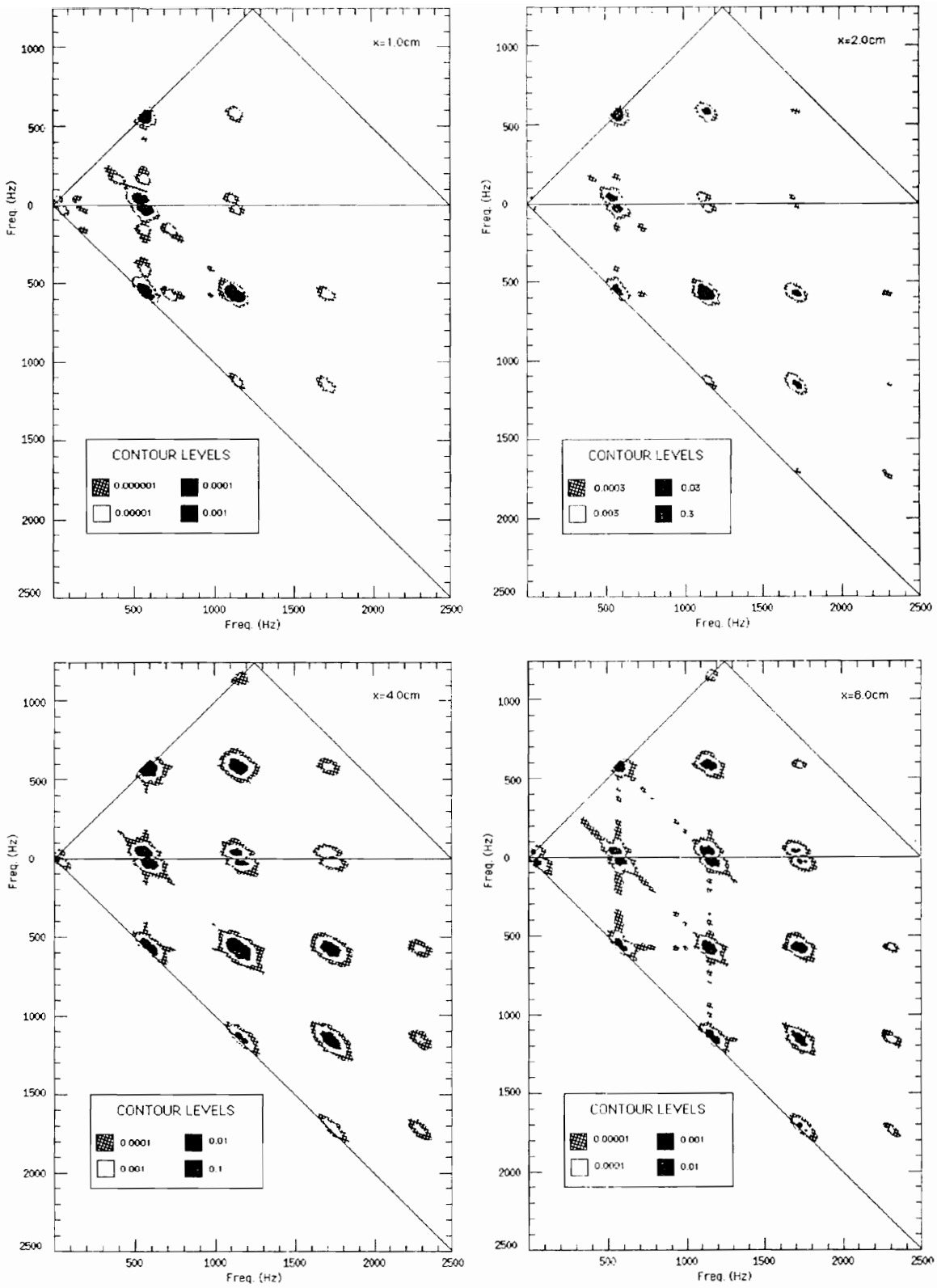

Figure 3.4. Contour plots of the magnitudes of the auto-bispectrum at the cross-stream location of maximum u'_{rms} at x=1.0, 2.0, 4.0, and 8.0cm (controlled case).

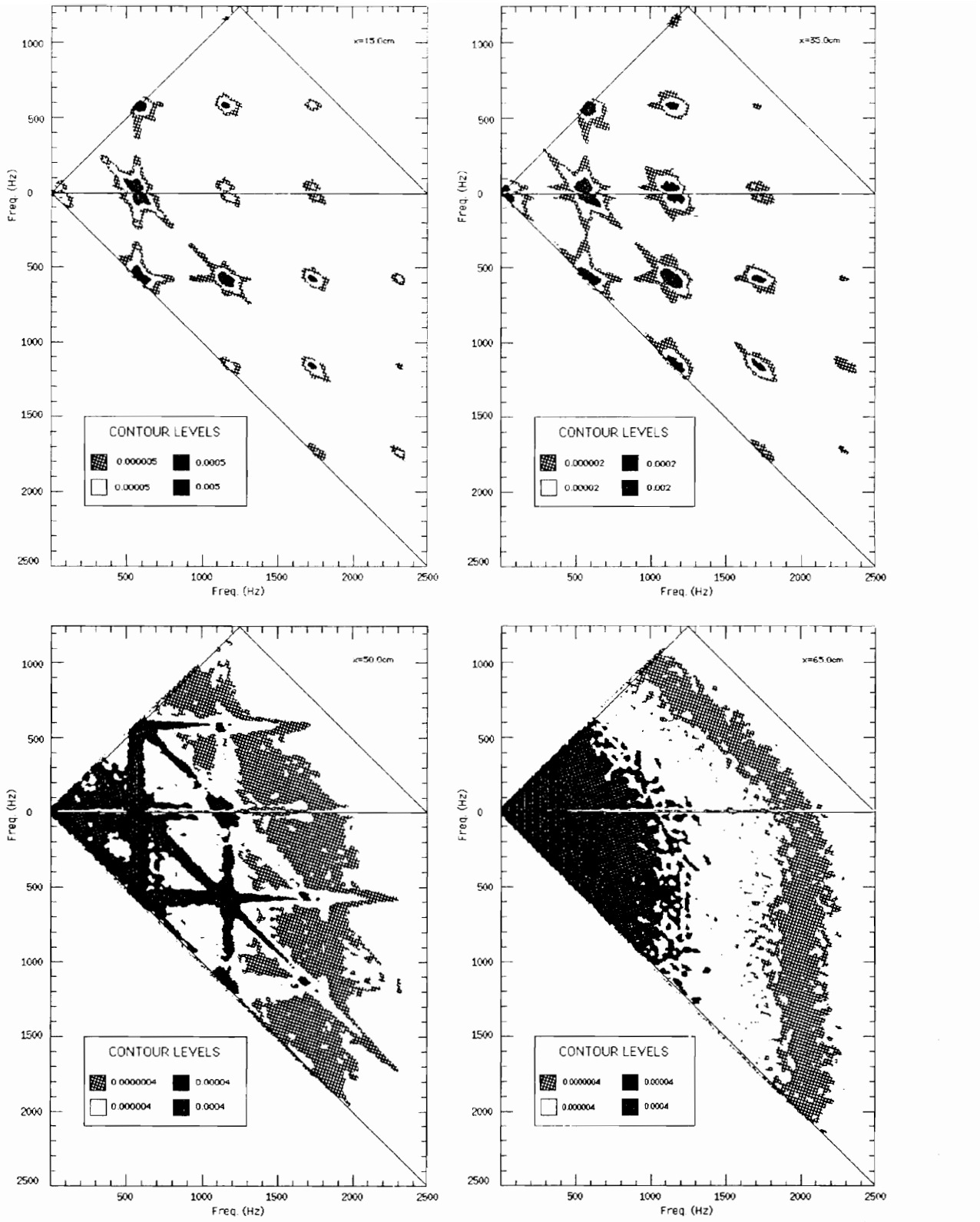

Figure 3.4 (cont'd). Contour plots of the magnitudes of the auto-bispectrum at the cross-stream location of maximum u'_{rms} at x=15.0, 35.0, 50.0, and 65.0cm (controlled case).

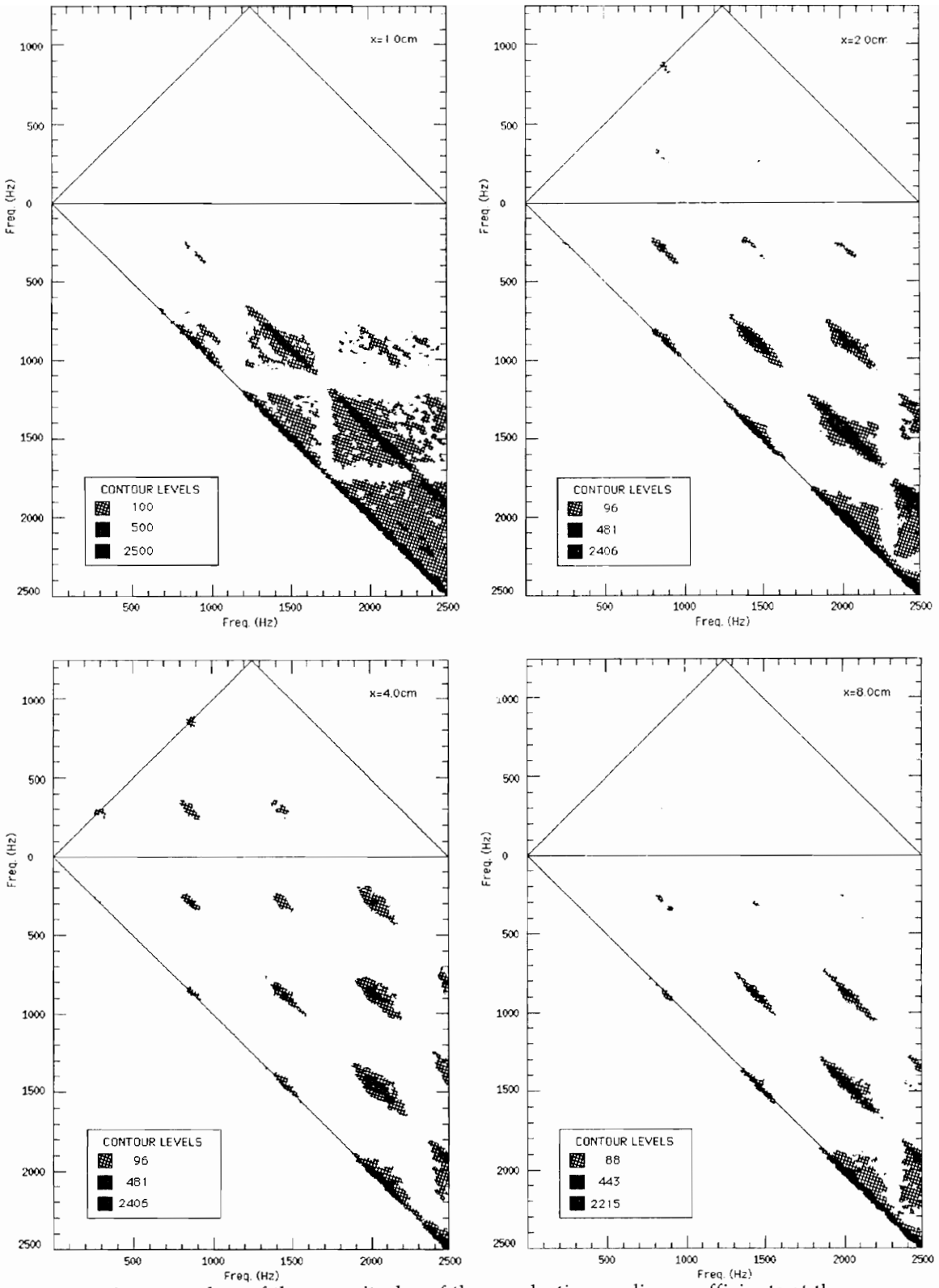

Figure 3.5. Contour plots of the magnitudes of the quadratic coupling coefficients at the cross-stream locaton of maximum u'_{rms} at x=1.0, 2.0, 4.0, and 8.0cm (controlled case).

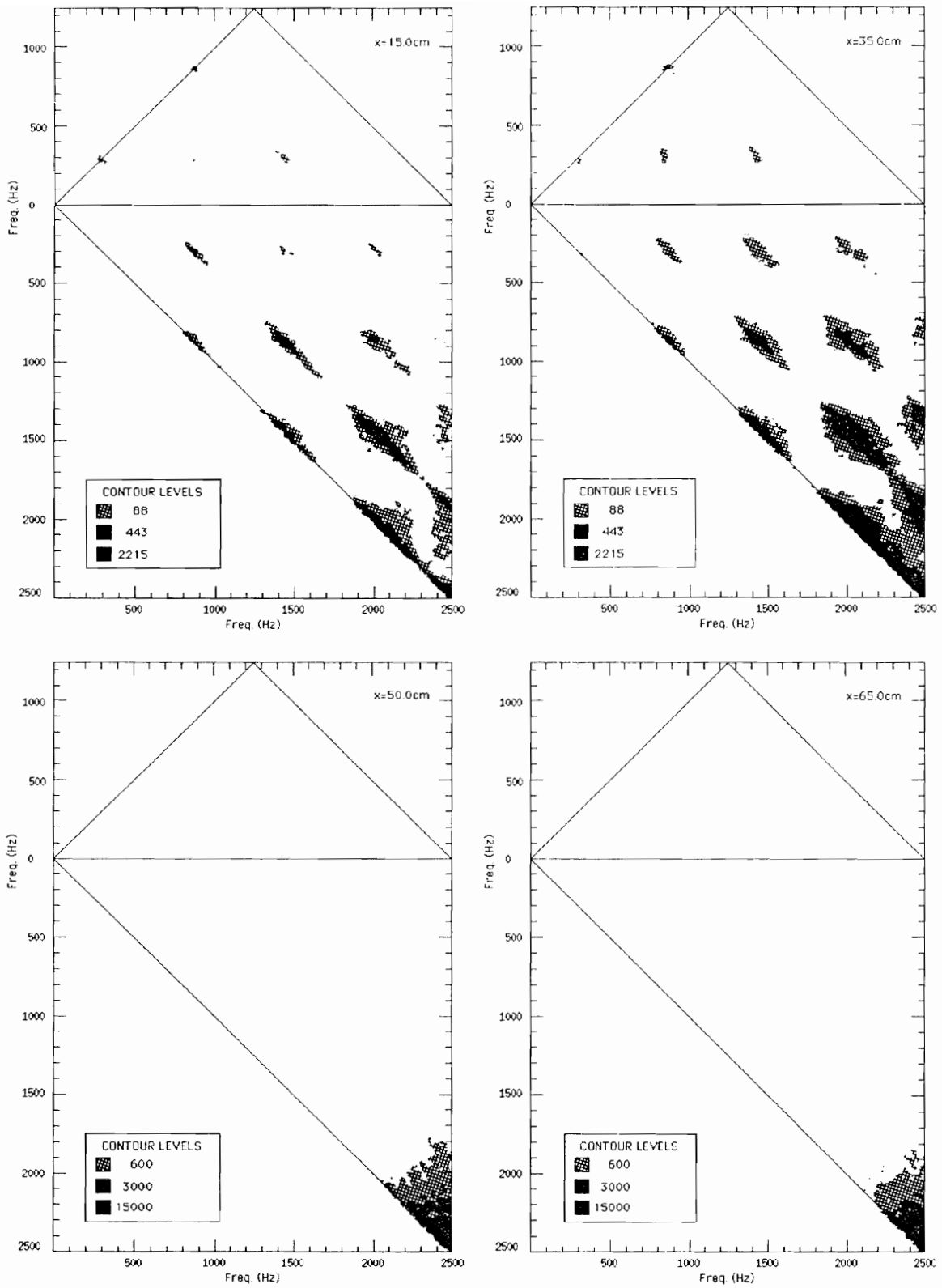

Figure 3.5 (cont'd). Contour plots of the magnitudes of the quadratic coupling coefficients at the cross-stream location of maximum u'_{rms} at x=15.0, 35.0, 50.0, and 65.0cm (controlled case).

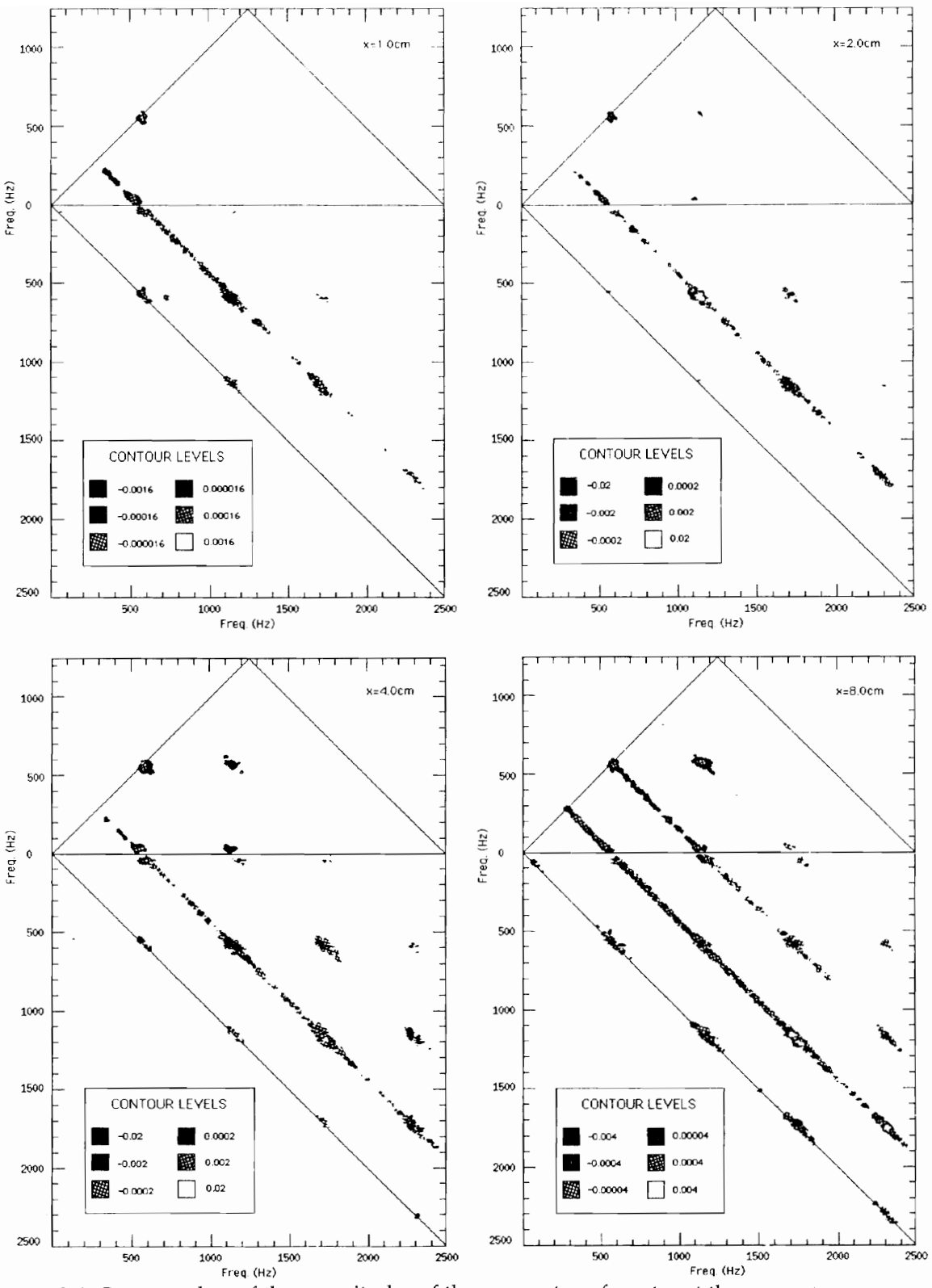

Figure 3.6. Contour plots of the magnitudes of the energy-transfer rates at the cross-stream location of maximum u'_{rms} at x=1.0, 2.0, 4.0, and 8.0cm (controlled case).

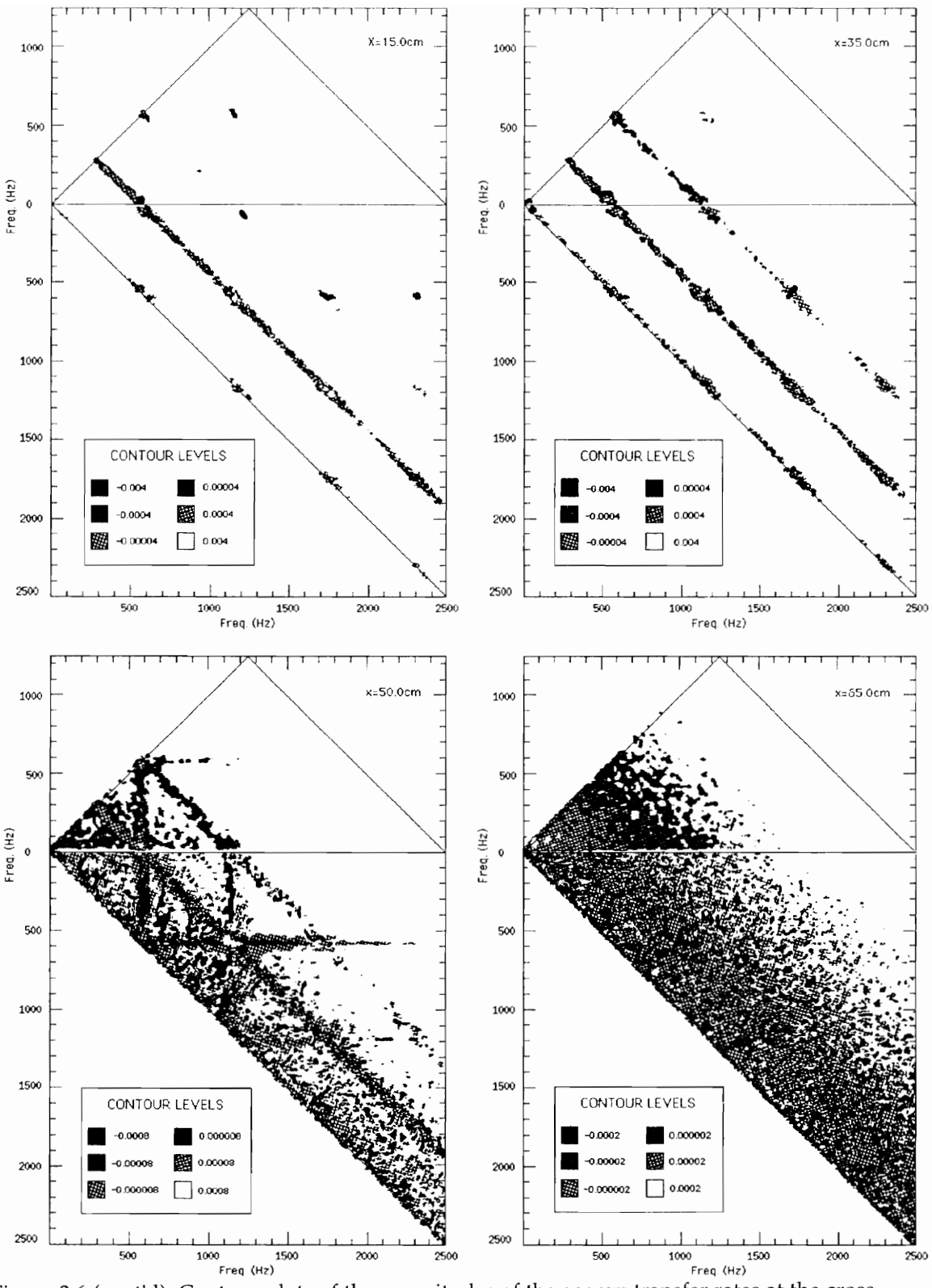

Figure 3.6 (cont'd). Contour plots of the magnitudes of the energy-transfer rates at the cross-stream location of maximum u'_{rms} at x=15.0, 35.0, 50.0, and 65.0cm (controlled case).

Chapter IV

Energy Cascading in a Natural Wake

In the previous chapter, the energy-cascading processes in the transition of a controlled plane wake were quantified. In those experiments, two small-amplitude instability modes of the initial wake were acoustically excited. Under those conditions, the two modes interact to generate a difference low-frequency component. This component was found to play an important role in the generation of sidebands and spectral filling of the valleys. Under natural conditions, with no preferred acoustic excitation, low-frequency amplification takes place randomly. In this chapter, energy-cascading processes that take place in the natural transition of a plane wake are quantified and compared to those that take place in controlled transition. A sequence of measurements of the power spectra, linear coherence, auto-bispectra, linear and quadratic coupling coefficients and quadratic energy-transfer rates are presented at four downstream locations. that represent the different stages of the transition. Differences and similarities between the controlled and natural cases are also pointed out.

4.1 *Spectral Energy Development in the Natural Wake*

The spectral energy distribution obtained from both sensors of the probe, at $x = 1.0, 4.0, 15.0$, and $50.0cm$ are given in figure 4.1. The energy spectrum at $x = 1.0cm$ shows the emergence of a band of dominant instabilities around the fundamental mode. Another band around the first harmonic also appears. By comparing the spectral energy distribution in both controlled (figure 3.1) and natural cases, one can notice that the bands around both the fundamental and first harmonic have lower energy levels in the natural case than in the controlled case. This indicates that the excitation of the instability modes not only increases their magnitudes but enhances their interactions.

By $x = 4.0cm$, the bands noticed at $x = 1.0cm$ show continuous growth and new bands around the second and third harmonics emerge. What is more important than the emergence of the harmonic bands is the emergence of the low-frequency components. By comparing with the spectra of the controlled transition (figure 3.1), one can notice that, while the second and third harmonic peaks are slightly larger in the controlled case, the energy content of all low-frequency modes with frequencies below $150Hz$ is larger in the natural case. It can also be noticed that the energy content of the sidebands and valleys in the natural case is larger than in the controlled one. This is of particular significance as the low-frequency components play an important role in the energy redistribution to the sidebands.

The role of these low-frequency modes can best be seen by examining the difference in the spectral energy content further downstream, at $x = 15.0cm$. A comparison between the two cases at this location shows that, while the peaks have about the same energy content in both cases, all other modes are significantly larger in the natural case

than in the controlled case (figure 3.1). This is also noticed at $x = 50.0cm$ where the energy content of the low-frequency components is still larger in the natural case.

4.2 *Nonlinear Spectral Energy-Transfer Mechanisms*

4.2.1 Bispectral Measurements and Analysis

Nonlinear wave coupling between the different spectral modes at $x = 1.0, 4.0, 15.0,$ and $50.0cm$ can be obtained from the auto-bispectra plots which are shown in figure 4.2. Table 4 shows the maximum values of the auto-bispectra at four different downstream locations.

Table 4. Auto-bispectrum maximum values

Downstream Location (cm)	Auto-bispectrum ($1/Hz^2$)
1.0	0.00015772
4.0	3.28877289
15.0	0.0358605
50.0	0.0041862

At $x = 1.0cm$, the largest coupling is between the band of frequency components centered around the fundamental mode and the low-frequency components. This differs from the excited case (figure 3.4) where large auto-bispectral values are measured between the excited modes and their first harmonics. At $x = 4.0cm$, the auto-bispectra look the same in both cases with one exception. The values of the auto-bispectra

between the fundamental mode, the instability modes surrounding the fundamental and low-frequency components are larger in the natural case. By $x = 15.0cm$, the bispectra plots in the natural transition show that the largest bispectra are those involving low-frequency components and modes that cover peaks as well as sidebands of the spectra. In contrast, the controlled case shows that coupling is highest between peaks at the fundamental mode, and its first and second harmonics. By $x = 50.0cm$ in natural transition, the largest coupling is along the lines that include the low-frequency bands; while in the controlled case, it is along lines that include the fundamental mode.

4.2.2 Quadratic Coupling Coefficients Measurements and Analysis

Measured quadratic coupling coefficients in the natural transition of the plane wake are given in figure 4.3. Table 5 shows the maximum values of the quadratic coupling coefficients at four different downstream locations. By comparing these measurements with those obtained in the controlled transition, the following conclusions could be drawn. In general, at all downstream locations, the coupling coefficients are highest between triplets of modes that fall in the valleys or at modes with highest frequencies. This implies that modes with the least amount of energy would have the highest coupling coefficients. As mentioned earlier, this is due to the sensitivity of these coefficients to the energy levels of the input and output modes. Thus, the highest measured magnitudes of the coupling coefficient does not necessarily reflect the largest energy transfer. These measurements are best shown in the energy transfer rates measurements that are discussed in the next section.

Table 5. Coupling coefficients maximum values

Downstream Location (cm)	Coupling Coefficients (Hz/mm)
1.0	5977.096716
4.0	23443.292620
15.0	6719.961697
50.0	32321.582555

4.2.3 Energy-Transfer Rates Measurements and Analysis

Measured values of the energy-transfer rates between all spectral components are given in figure 4.4. Table 6 shows the maximum values of the energy-transfer rates taken at four different downstream locations. The results show important differences between the natural and acoustically excited transitions. At $x = 1.0cm$, the measurements show that the intensity of quadratic energy-transfer rates is much lower in the natural case than in the excited case. This explains why the level of energy of the peaks and low-frequency components is lower in the natural case than in the excited case. At $x = 4.0cm$, the measurements show that the most significant energy-transfer rates are those between the fundamental mode and the first harmonic. Lower levels of quadratic energy-transfer rates are measured between triplets of modes that include the fundamental mode, low-frequency components and sidebands and other triplets that include the higher harmonics. At $x = 15.0cm$, the measurements show that the largest energy-transfer rates is between triplets of modes that include the low-frequency components. These are significantly different from the controlled transition measurements which show the largest energy-transfer rates between triplets of modes

that include the fundamental mode. At $x = 50.0cm$, the measurements stress again the role of the low-frequency modes in energy transfer to other components.

Table 6. Energy-transfer rate maximum values

Downstream Location (cm)	Energy-Transfer Rates ($1/Hz.mm$)
1.0	-0.000093332
4.0	-0.427353758
15.0	0.002398258
50.0	-0.001407629

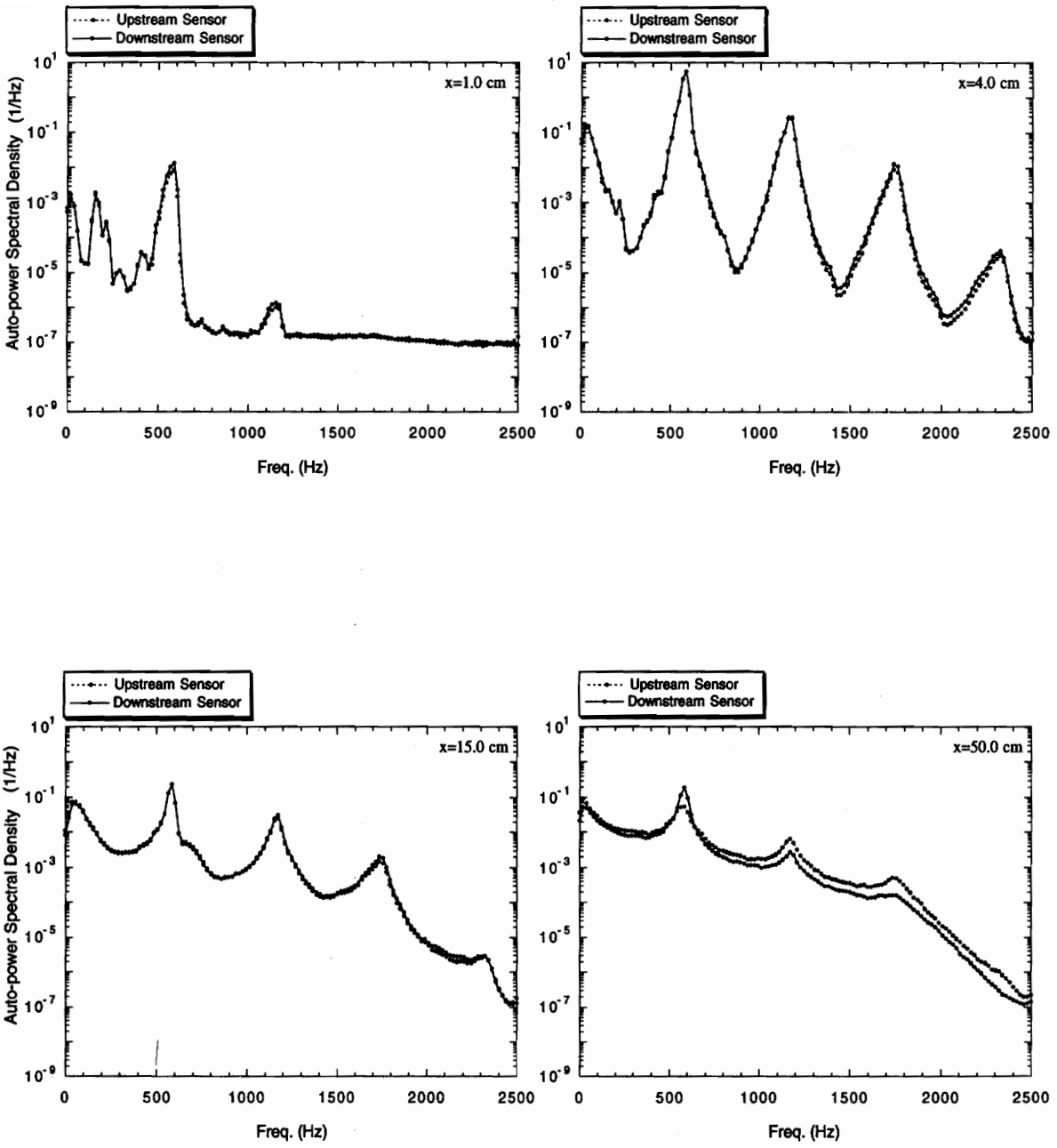

Figure 4.1. Spectral energy distribution of the velocity fluctuations at the cross-stream location of maximum u'_{rms} at x=1.0, 4.0, 15.0, and 50.0cm (natural case).

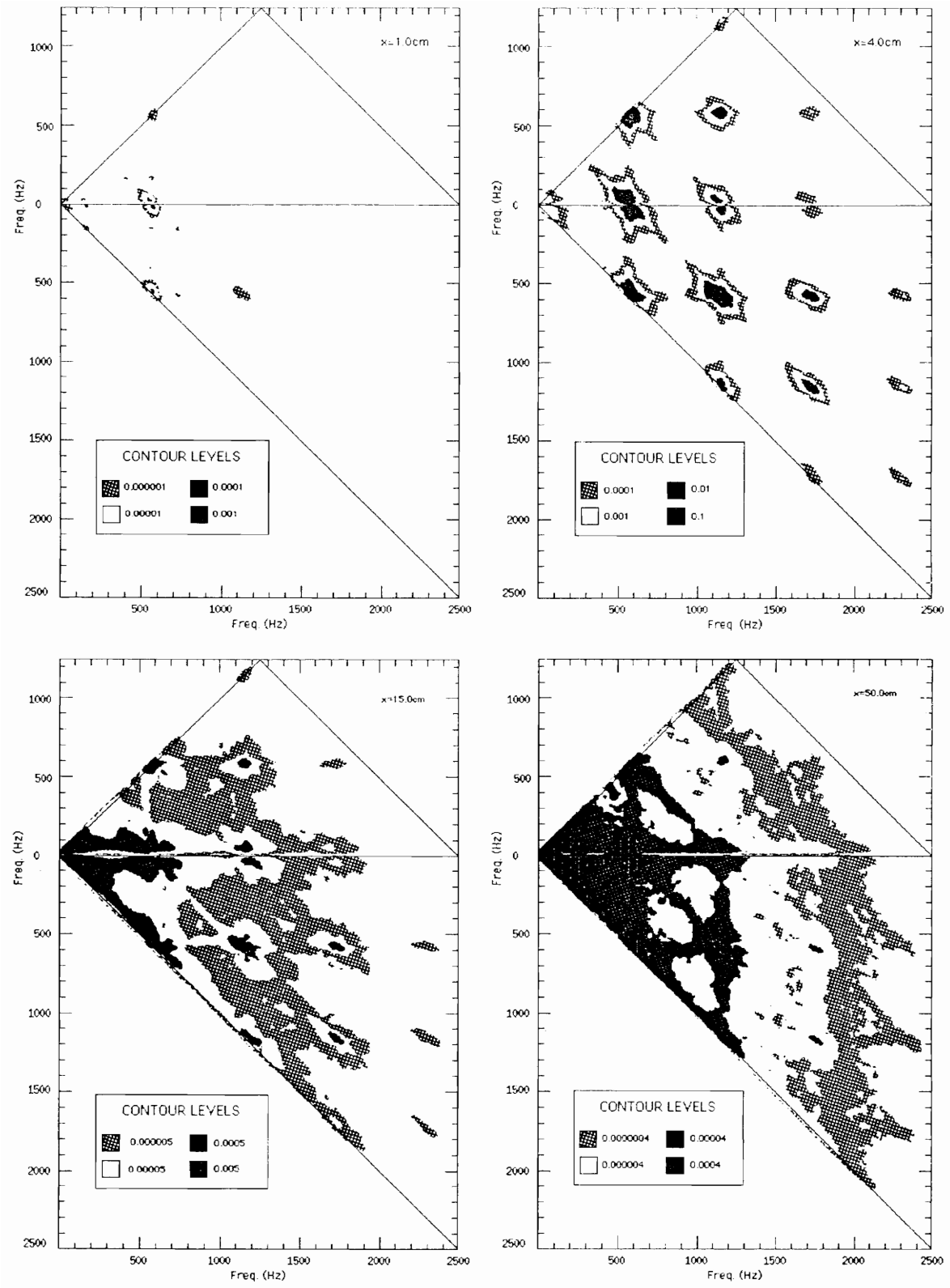

Figure 4.2. Contour plots of the magnitudes of the auto-bispectrum at the cross-stream location of maximum u'_{rms} at x=1.0, 4.0, 15.0, and 50.0cm (natural case).

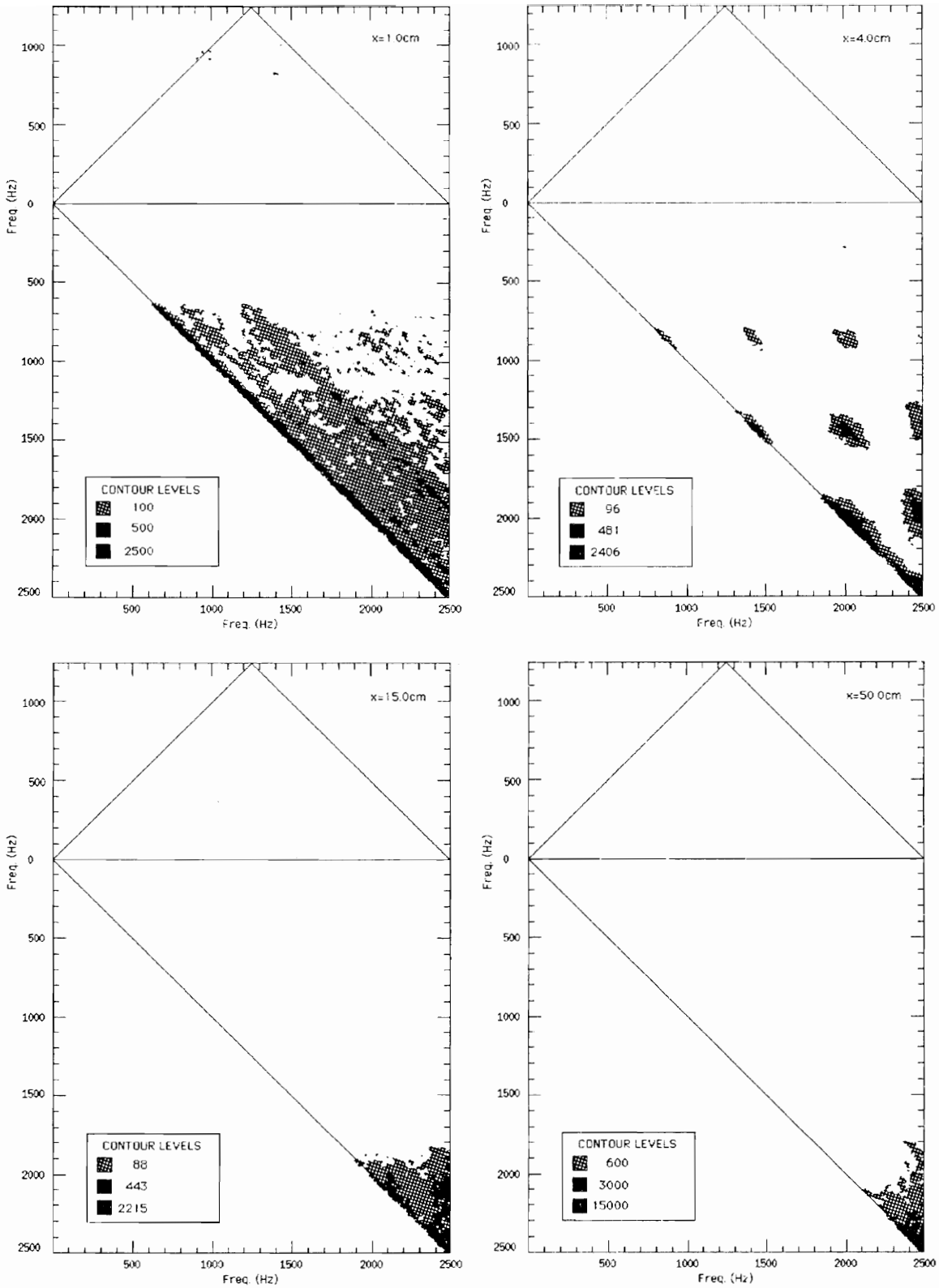

Figure 4.3. Contour plots of the magnitudes of the quadratic coupling coefficients at the cross-stream location of maximum u'_{rms} at x=1.0, 4.0, 15.0, and 50.0cm (natural case).

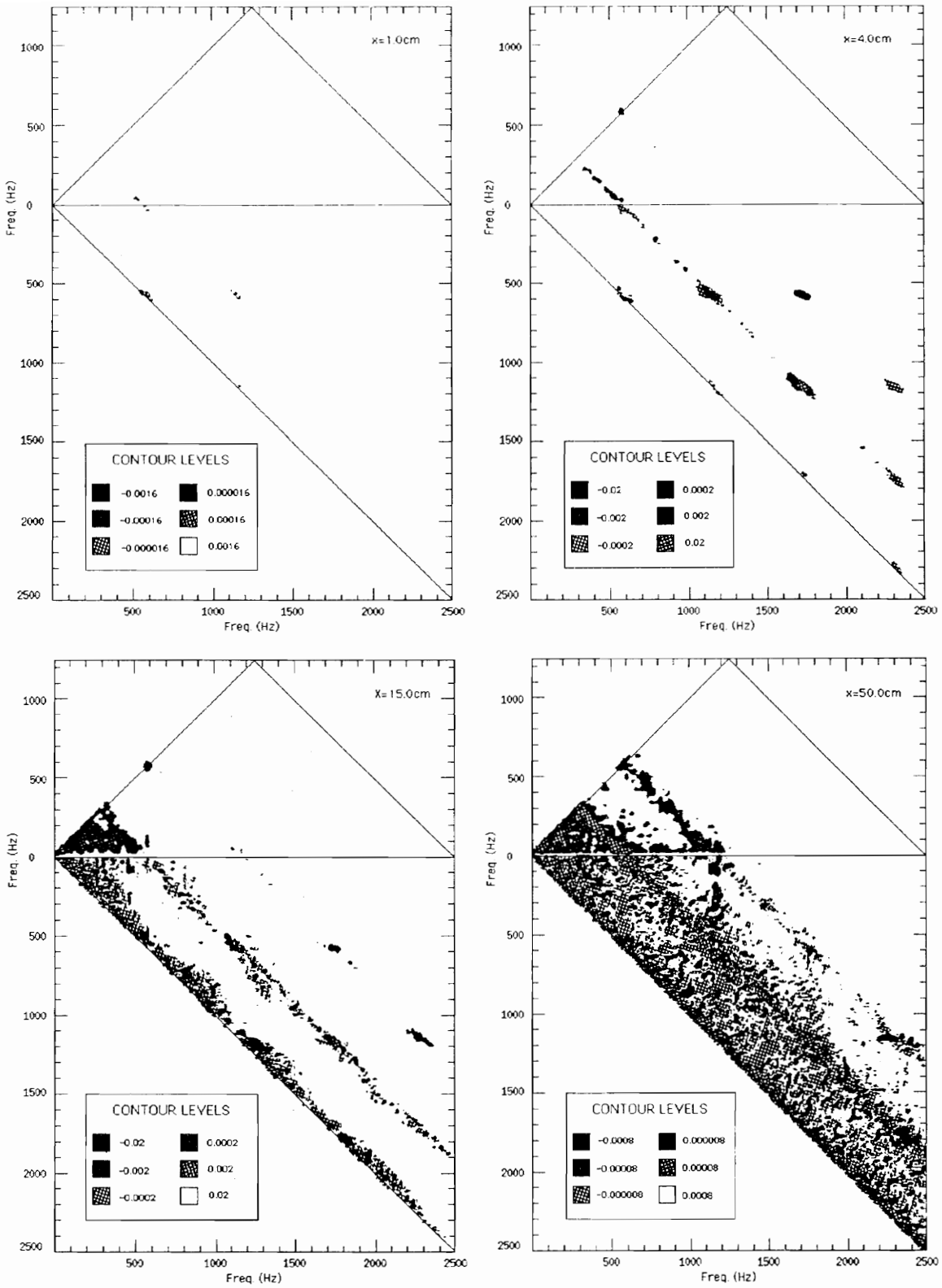

Figure 4.4. Contour plots of the magnitudes of the energy transfer-rates at the cross-stream location of maximum u'_{rms} at x=1.0, 4.0, 15.0, and 50.0cm (natural case).

Chapter V

Summary and Conclusions

The objective of the work presented in this study is to experimentally quantify the energy-cascading processes in the natural and controlled transition of a plane wake. Quantities such as the coupling coefficients and transfer functions, which can be related to the Navier-Stokes equations, along with the auto-bispectra have been measured to quantify these processes. In summary, the results lead to the following conclusions:

- The quadratic energy-transfer rates between the spectral modes are dependent on the phases and magnitudes of both the coupling coefficients as well as the auto-bispectrum. A look at the magnitude of the energy-transfer rates shows that they are significantly different from those of the auto-bispectra (or auto-bicoherence) and those of the quadratic coupling coefficients.

- The largest quadratic coupling coefficient measurements do not necessarily represent the largest energy-transfer rate, because of the sensitivity of these coefficients to the energy level of the input and output modes.

- The results show that in both natural and controlled transitions the nonlinear interactions between instability modes play a dominant role in the energy transfer to the harmonic bands and to the low-frequency components. The low-frequency components then play an important role in energy transfer to the sidebands and valleys between the peaks, leading to the final breakdown of the flow into turbulence.

- While the underlying nonlinear dynamics in both controlled and natural transitions are similar (previous conclusion), the characteristics of the transition are different. In the controlled case, the double excitation enhances the generation of the harmonic band structures and one low-frequency difference component. This is followed by an extended period of "equilibrium", between $x = 8.0$ and $x = 35.0cm$, where the nonlinear energy-transfer rates show a slow filling of the spectral valleys. In contrast, the random nature of the wave excitation in the natural case causes energy transfer to a band of low-frequency components rather than stressing the one difference component as in the controlled case. This leads to lower but wider energy-transfer rates to the sidebands which results in a spectra in the natural case that differ dramatically from those obtained in the controlled case.

The above results showed that measurements of energy-transfer rates in the natural and controlled transitions of a plane wake provided new insights into the nonlinear dynamics that govern these transitions. Furthermore, the results enhanced our understanding of the different spectral quantities and how they can be used to examine a nonlinear dynamic phenomenon.

References

1. Gaster, M. **Prog. Aero. Scie. 6** (1965)

2. Gertshenstein, S.Ya., Sukhorukov, A.N., and Shkadov, V.Ya. "Nonlinear oscilations in a two-dimensional wake." **Fluid Dynamics 12** (1977).

3. Hajj, M.R., Miksad, R.W. and Powers, E.J. "Subharmonic growth by paramatric resonance." **J. Fluid Mech 236** 385-413 (1992).

4. Jones, F.L., "An Experimental study of nonlinear wave interaction and modulations during transition of a sysmmetric wake". **Thesis** UTA (1983).

5. Jones, F.L., Ritz, C.P., Miksad, R.W., Powers, E.J. and Solis, R.S. "Measurements of the local wavenumber and frequency spectrum in a plane wake". **Exps. in Fluids 6, 365-372** (1988).

6. Kim, Y.C., Powers, E.J., "A digital method of modeling quadratically nonlinear systems with a general random input." **I.E.E.E. Trans. on Acoustics. 36** 1758-1769 (1988).

7. Kim, Y.C., Beall, J.M., Powers, E.J., and Miksad, R.W., "Bispectrum and nonlinear wave coupling." **Phys. Fluids 23,** (1980), 258-263.

8. Kim, Y.C. and Powers, E.J. "Wave modulation in a nonlinear dispersive medium." **Phys. Fluids 23,** (1980), 2250-2257.

9. Kim, Y.C. and Powers, E.J. "Digital bispectral analysis and its applications to nonlinear wave interactions." **I.E.E.E. Trans. Plasma Sci. PS-7,** 2, (1979), 120-131.

10. Kraichnan, R. **Phys. of Fluids, 10** (1967)

11. Miksad, R. W., Jones, F. L., Powers, E. J., Kim, Y. C., and Khadra, L. "Experiments on the role of amplitude and phase modulations during transition to turbulence" **J. Fluid Mech. 123** (1982), 1-29.

12. Miksad, R.W., Jones, F.L, Ritz, C.P., and Powers, E.J. "The role of nonlinear wave wave interactions in laminar-turbulent transition." **Arch. Mech., 39** (1987) 177-205.

13. Motohashi, T. "A higher-order nonlinear interaction among spectral components." **Phs. Fluids 22** 6 (1979), 1212-1213.

14. Nayfeh, A.H. and Bozatli, A.N "Nonlinear interactions of two waves in boundary-layer flows." **Phys. Fluids 23** (1980), 448-458.

15. Ritz, Ch.P., Powers, E.J., and Bengtson, R.D. "Experimental measurements of three-wave coupling and energy cascading." **Phys. Fluids** 153-163 (1989).

16. Ritz, Ch.P., Powers, E.J., Miksad, R.W., And Solis, R.S, "Nonlinear spectral dynamics of transitioning flow" **Phys. Fluids** (1988) 3577-3588

17. Sato, H. "An experimental study of non-linear interaction of velocity fluctuations in the transition region of a two-dimensional wake." **J. Fluid Mech. 44** (1970), 741-765.

18. Sato, H. and Saito, H. "Fine-structure of energy spectra of velocity fluctuations in the transition region of a two-dimensional wake." **J. Fluid Mech. 67** (1975), 539-559.

Appendices

Appendix A

Methodology Used to Estimate the Linear and Quadratic Coupling Coefficients

The wave coupling equation is written as:

$$\frac{\partial \mathrm{X}(f,x)}{\partial x} = \Lambda_L(f)\mathrm{X}(f,x) + \frac{1}{2}\sum_{f_i,f_j}\Lambda_Q(f_i,f_j)\mathrm{X}(f_i,x)\mathrm{X}(f_j,x) \qquad (A.1)$$

Where $\Lambda_L(f)$ and $\Lambda_Q(f_i,f_j)$ are the linear and quadratic coupling coefficients respectively. The linear coupling coefficient is expressed as follows:

$$\Lambda_L(f) = \gamma_p(f) + i\omega_p \qquad (A.2)$$

where $\gamma_p(f)$ is the growth rate and $\omega_p(f)$ is the dispersion relation. Introducing a finite difference scheme to estimate the linear growth rate $\gamma_p(f)$, the dispersion relation $\omega_p(f)$, and the quadratic coupling $\Lambda_Q(f_i,f_j)$, one can write

$$\frac{\partial X(f,x)}{\partial x} = \lim_{\Delta \to 0} \left(\frac{|X(f,x+\Delta x)| - |X(f,x)|}{\Delta x} \frac{1}{|X(f,x)|} \right.$$

$$\left. + i \frac{\phi(f,x+\Delta x) - \phi(f,x)}{\Delta x} \right) X(f,x) \qquad (A.3)$$

where $X(f,x) = |X(f,x)| e^{i\phi(f,x)}$ substituting A.3 in the wave coupling equation, one can solve for an output spectrum $X(f,x+\Delta x)$, which gives

$$X(f,x+\Delta x) = \frac{\Lambda_L(f)\Delta x + 1 - i[\phi(f,x+\Delta x) - \phi(f,x)]}{e^{-i[\phi(f,x+\Delta x) - \phi(f,x)]}} X(f,x)$$

$$+ \frac{1}{2} \sum_{f_i, f_j}^{m} \frac{\Lambda_Q(f_i,f_j)\Delta x}{e^{-i[\phi(f,x+\Delta x) - \phi(f,x)]}} X(f_i,x) X(f_j,x) \qquad (A.4)$$

where

$\Lambda_L(f) = \gamma_p(f) + i\omega_p(f)$, and $f = f_i \pm f_j$ always. The above equation can also be written as

$$Y(f) = L(f)X(f) + \sum_{f_i} \sum_{f_j} Q(f_i,f_j) X(f_i) X(f_j) \qquad (A.5)$$

Where

$$Y(f) = X(f, x+\Delta x) \qquad (A.6)$$

$$L(f) = \frac{\Lambda_L(f)\Delta x + 1 - i[\phi(f,x+\Delta x) - \phi(f,x)]}{e^{-i[\phi(f,x+\Delta x) - \phi(f,x)]}} \qquad (A.7)$$

$$Q(f_i, f_j) = \frac{1}{2} \sum_{f_i f_j}^{m} \frac{\Lambda_Q(f_i, f_j)\Delta x}{e^{-i[\phi(f,x+\Delta x)-\phi(f,x)]}} \tag{A.8}$$

where $f = f_i \pm f_j$, and $L(f)$ and $Q(f)$ are the linear and quadratic transfer functions respectively. From the spatial distance between the two measuring points, their phase shift, and energy transfer functions, one obtains an estimate of the coupling coefficients. The methodology used to solve for the transfer functions is discussed in appendix B.

Appendix B

Methodology Used to Estimate the Linear and Quadratic Transfer Functions

The input/output linear and quadratic model, obtained in appendix A, in discrete frequency format is expressed as follows:

$$Y(f) = L(f)\mathrm{X}(f) + \sum_{f_i}\sum_{f_j} Q(f_i, f_j)\mathrm{X}(f_i)\mathrm{X}(f_j) \qquad (B.1)$$

where $L(f)$ and $Q(f_i, f_j)$, respectively, are the linear and the quadratic transfer functions over a discrete frequency band, and $f = f_i \pm f_j$. $\mathrm{X}(f)$ and $Y(f)$ are the complex Fourier amplitudes of the velocity signals with frequency f obtained at the upstream and downstream sensors of the probe respectively.

In order to solve for the two unknowns, namely linear and quadratic transfer functions, two equations are needed. To do that we multiply equation (B.1) once by $\mathrm{X}^*(f)$ and once by $\mathrm{X}^*(f_k), \mathrm{X}^*(f_l)$. The resulting set of equations is given by:

$$E[Y(f)X^*(f)] = L(f)E[|X(f)|^2] + \sum_{\substack{f_i \\ f=f_i \pm f_j}} \sum_{f_j} Q(f_i,f_j)E[X(f_i)X(f_j)X^*(f)] \qquad (B.2)$$

$$E[Y(f)X^*(f_k)X^*(f_l)] = L(f)E[X^*(f_k)X(f_l)]$$

$$+ \sum_{\substack{f_i \\ f=f_i \pm f_j}} \sum_{\substack{f_j \\ f_j=f_k \pm f_l}} Q(f_i,f_j)E[X(f_i)X(f_j)X^*(f_k)X^*(f_l)] \qquad (B.3)$$

where always $f = f_i \pm f_j = f_k \pm f_l$ and $E[...]$ denotes an expected value. General solution for L and Q requires solving equations (3) and (4) simultaneously which involves very complicating mathematics. For the case of a zero-mean Gaussian input, the auto bispectrum is zero and the linear and quadratic transfer functions can be computed independently. The solution is then given by:

$$L(f) = \frac{X^*(f)Y(f)}{|X(f)|^2}, \qquad (B.4)$$

$$Q(f_i,f_j) = \frac{X^*(f_i)X^*(f_j)Y(f)}{2|X(f_i)|^2|X(f_j)|^2|X(f)|^2}, \qquad (B.5)$$

where $X^*(f_i)X^*(f_j)Y(f)$ is the cross bispectra, $X^*(f)Y(f)$ is the cross spectra, and $X^*(f)X(f)$ is the auto power spectra.

For non-Guassian input, an explicit solution of the above equation is rather complex, and a digital solution is more feasible. The advantage of the digital solution

is that it is generic and simple for implementation. In vector notation equations (B.2) and (B.3) are written as:

$$\begin{bmatrix} E[Y(f)X^*(f)] \\ E[Y(f)X^*(f_k)X^*(f_l)] \end{bmatrix} =$$

$$\begin{bmatrix} E[X(f)X^*(f)] & E[X(f)X^*(f_k)X^*(f_l)] \\ E[X(f_i)X(f_j)X^*(f)] & E[X(f_i)X(f_j)X^*(f_k)X^*(f_l)] \end{bmatrix} \begin{bmatrix} L(f) \\ Q(f_i,f_j) \end{bmatrix} \qquad (B.6)$$

The solution of the above system in terms of $L(f)$ and $Q_{(f_i,f_j)}$ is then given by:

$$\begin{bmatrix} L(f) \\ Q(f_i,f_j) \end{bmatrix} =$$

$$\begin{bmatrix} E[X(f)X^*(f)] & E[X(f)X^*(f_k)X^*(f_l)] \\ E[X(f_i)X(f_j)X^*(f)] & E[X(f_i)X(f_j)X^*(f_k)X^*(f_l)] \end{bmatrix}^{-1} \begin{bmatrix} E[Y(f)X^*(f)] \\ E[Y(f)X^*(f_k)X^*(f_l)] \end{bmatrix} \qquad (B.7)$$

To illustrate this expression, we expand the above system over frequency index of 10 as follows:

$$\begin{bmatrix} L(f_{10}) \\ Q(f_{10},f_0) \\ Q(f_9,f_1) \\ Q(f_8,f_2) \\ Q(f_7,f_3) \\ \vdots \\ Q(f_0,f_{10}) \end{bmatrix} =$$

$$\begin{bmatrix} |X(f_{10})|^2 & X(f_{10})X^*(f_{10})X^*(f_0) & X(f_{10})X^*(f_9)X^*(f_1) & \cdots & X(f_{10})X^*(f_0)X^*(f_{10}) \\ X(f_{10})X(f_0)X^*(f_{10}) & |X(f_{10})|^2|X(f_0)|^2 & X(f_{10})X(f_0)X^*(f_9)X^*(f_1) & \cdots & X(f_0)X(f_{10})X^*(f_0)X^*(f_{10}) \\ X(f_9)X(f_1)X^*(f_{10}) & X(f_9)X(f_1)X^*(f_{10})X^*(f_0) & |X(f_9)|^2|X(f_1)|^2 & \cdots & X(f_9)X(f_1)X^*(f_0)X^*(f_{10}) \\ X(f_8)X(f_2)X^*(f_{10}) & X(f_8)X(f_2)X^*(f_{10})X^*(f_0) & X(f_8)X(f_2)X^*(f_9)X^*(f_1) & \cdots & X(f_8)X(f_2)X^*(f_0)X^*(f_{10}) \\ X(f_7)X(f_3)X^*(f_{10}) & X(f_7)X(f_3)X^*(f_{10})X^*(f_0) & X(f_7)X(f_3)X^*(f_9)X^*(f_1) & \cdots & X(f_7)X(f_3)X^*(f_0)X^*(f_{10}) \\ \vdots & \vdots & \vdots & & \vdots \\ X(f_0)X(f_{10})X^*(f_{10}) & X(f_0)X(f_{10})X^*(f_{10})X^*(f_0) & X(f_0)X(f_{10})X^*(f_9)X^*(f_1) & & |X(f_{10})|^2|X(f_0)|^2 \end{bmatrix}^{-1}$$

$$\begin{bmatrix} Y(f_{10})X^*(f_{10}) \\ Y(f_{10})X^*(f_{10})X^*(f_0) \\ Y(f_{10})X^*(f_9)X^*(f_1) \\ Y(f_{10})X^*(f_8)X^*(f_2) \\ Y(f_{10})X^*(f_7)X^*(f_3) \\ \vdots \\ Y(f_{10})X^*(f_0)X^*(f_{10}) \end{bmatrix} \qquad (B.8)$$

In order to validate our results, we obtained the linear and quadratic transfer function. The input-output relation given by Kim & Powers [1988] as:

$$y(t) = -0.64x(t) + x(t-2) + 0.9x^2 + x^2(t-1) \qquad (B.9)$$

For this relation, the transfer functions are given explicitly as:

$$L(f) = -0.64 + e^{-i4\pi f} \tag{B.10}$$

$$Q(f_i, f_j) = 0.9 + e^{-i4\pi(f_i + f_j)} \tag{B.11}$$

Estimate of the transfer functions were also applying the above digital technique analysis to a set of data that exhibits an exponential behavior. This set was retrieved from IMSL routine, namely DREXP as a source of exponential data. Each input/output data record consisted of 65536 sample point of length, and was divided into 1024 segment with each segment contained 64 data points.

Figure B.1 shows a comparison between the linear transfer function given in equation (B.10) and the estimated one using the analysis of Kim and Powers [1988]. It is important to note the estimated linear transfer function varies with the number of averages. For 32 averages, estimate of the linear transfer does not match that obtained from equation (B.10). For 64 averages, the transfer function starts to show some feature of the true values with some error. The error declines significantly as the number of averages is increased to 512. This shows that the number of realizations should be adequate for estimating the linear and quadratic transfer function.

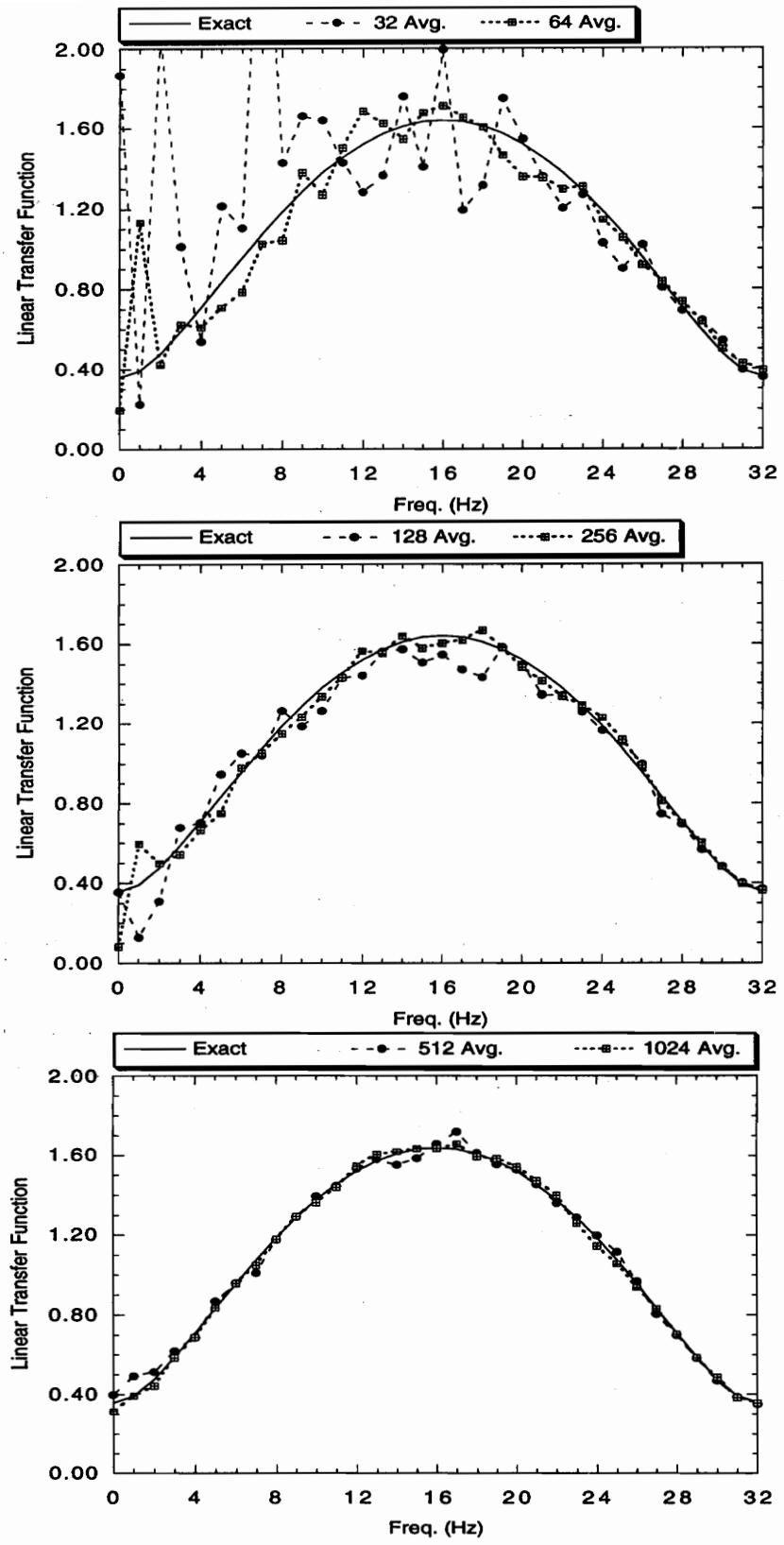

Figure B.1. Linear transfer function obtained from the digital analysis with different number of averages

Vita

Isam Mustafa Janajreh was born on February 14, 1966 in Zarka, Jordan. In 1984, after getting his high-school diploma from Zarka, he enrolled in Yarmouk University in Irbid, Jordan in Mechanical Engineering. Two years later, he joined the College of Engineering and Science of Jordan University of Science & Technology (JUST) and graduated in 1989. After graduation, he worked as a field engineer with the Jordan Port Corporations.

In fall 1990 he enrolled in the College of Engineering and received a Master of Science in Mechanical Engineering at Virginia Polytechnic Institute & State University. a Master of Science in Mechanical Engineering at Virginia Polytechnic In the spring of 1993 he entered the graduate program in the Department of Engineering Science and Mechanics at VPI&SU. Currently, he is working towards the Ph.D. in the Department of Engineering Science and Mechanics at VPI&SU.

Isam M. Janajareh